Article

Two broadly conserved families of polyprenyl-phosphate transporters

https://doi.org/10.1038/s41586-022-05587-z

Received: 2 March 2022

Accepted: 23 November 2022

Published online: 30 November 2022

Check for updates

Ian J. Roney[1] & David Z. Rudner[1]✉

Peptidoglycan and almost all surface glycopolymers in bacteria are built in the cytoplasm on the lipid carrier undecaprenyl phosphate (UndP)[1–4]. These UndP-linked precursors are transported across the membrane and polymerized or directly transferred to surface polymers, lipids or proteins. UndP is then flipped to regenerate the pool of cytoplasmic-facing UndP. The identity of the flippase that catalyses transport has remained unknown. Here, using the antibiotic amphomycin that targets UndP[5–7], we identified two broadly conserved protein families that affect UndP recycling. One (UptA) is a member of the DedA superfamily[8]; the other (PopT) contains the domain DUF368. Genetic, cytological and syntenic analyses indicate that these proteins are UndP transporters. Notably, homologues from Gram-positive and Gram-negative bacteria promote UndP transport in *Bacillus subtilis*, indicating that recycling activity is broadly conserved among family members. Inhibitors of these flippases could potentiate the activity of antibiotics targeting the cell envelope.

Polyprenyl phosphates are universal carriers of sugars and glycopolymers across membranes in all domains of life[1–4]. In bacteria, the 55-carbon isoprenoid UndP (also known as C55-P) is used to transport most glycopolymers across the cytoplasmic membrane including peptidoglycan precursors, O-antigens of lipopolysaccharide, teichoic acids and capsular polysaccharides. UndP also ferries sugars and oligosaccharides across the membrane that are used to glycosylate lipid A of lipopolysaccharide, teichoic acids and surface proteins (Extended Data Fig. 1). In eukaryotes and archaea, the polyprenyl phosphate dolichol phosphate (DolP) transports oligosaccharides across the membranes of the endoplasmic reticulum and the archaeal cytoplasmic membrane, respectively[1,2]. These DolP-linked sugars are then used to decorate membrane-anchored and secreted proteins. In all cases, the lipid carrier must be recycled through transport across the membrane. The flippases that catalyse polyprenyl-phosphate transport are among the last unknown enzymes in these pathways.

Bacterial cell wall biogenesis, the target of some of the most effective antibiotics, exemplifies these glycopolymer synthesis pathways[9] (Fig. 1). A series of cytoplasmic enzymatic steps generate the peptidoglycan precursor lipid II, a disaccharide pentapeptide linked to undecaprenyl pyrophosphate (UndPP). Lipid II is then flipped to the outer leaflet of the cytoplasmic membrane where the muropeptide is polymerized and crosslinked into the cell wall meshwork. The UndPP product is dephosphorylated and the resulting UndP is flipped to the inner leaflet to complete the lipid II cycle (Fig. 1). During exponential growth, a bacterium contains about 10^5 UndP molecules that are thought to ferry a similar number of peptidoglycan precursors across the cytoplasmic membrane every minute, suggesting that each lipid carrier is reused multiple times per cell cycle for peptidoglycan synthesis alone[10,11]. De novo synthesis of UndP maintains the pool size during growth whereas recycling is the primary source for surface polymer biogenesis. Here we define two broadly conserved families of flippases that catalyse UndP transport in bacteria and could function to recycle DolP in eukaryotes and archaea.

Identification of UndP transporters

To screen for potential UndP flippases, we took advantage of the antibiotic amphomycin and its derivative MX2401 (refs. [5–7]) that bind the phosphate on UndP. As these cyclic lipopeptides are unlikely to cross the membrane, they are thought to bind outward-facing UndP preventing its recycling and thus inhibit peptidoglycan synthesis. We reasoned that overexpression of an UndP transporter would provide resistance to these antibiotics. We generated a *B. subtilis* transposon library with a strong outward-facing promoter[12] and plated the library on lysogeny broth agar supplemented with MX2401 at concentrations above the minimum inhibitory concentration (MIC). The colonies were pooled and the transposon insertion sites were mapped by transposon sequencing (Tn-seq). Transposon insertions were significantly overrepresented at a single region of the genome, and in all cases the outward-facing promoter faced the uncharacterized gene *yngC* (Fig. 2a). Overexpression of *yngC* in *B. subtilis* increased the MIC of MX2401 by >16-fold (Fig. 2b), validating our findings. Furthermore, deletion of *yngC* reduced the MIC fourfold (Fig. 2b). These data suggest that YngC functions in UndP transport.

YngC is a member of the DedA superfamily, a broadly conserved but poorly understood family of membrane proteins found in all domains of life[8]. The AlphaFold-predicted structure of YngC resembles the structure of membrane transporters with membrane re-entrant loops on either side of the lipid bilayer[13] (Extended Data Fig. 2a). A conserved pair of arginines in one of these loops is required for MX2401 resistance (Extended Data Fig. 2b and Supplementary Fig. 2a) and could function in phosphate binding. Notably, one of the promoters of *yngC* is regulated by the extracytoplasmic function sigma factor σ^M (ref. [14]; Extended Data Fig. 2e–g). This transcription factor is induced under conditions that trap UndP-linked intermediates and reduce the cellular pools of the lipid carrier[15]. Consistent with a role for σ^M in regenerating this pool, a *sigM* mutant or a deletion of the σ^M-binding site in the *yngC*

[1]Department of Microbiology, Harvard Medical School, Boston, MA, USA. ✉e-mail: rudner@hms.harvard.edu

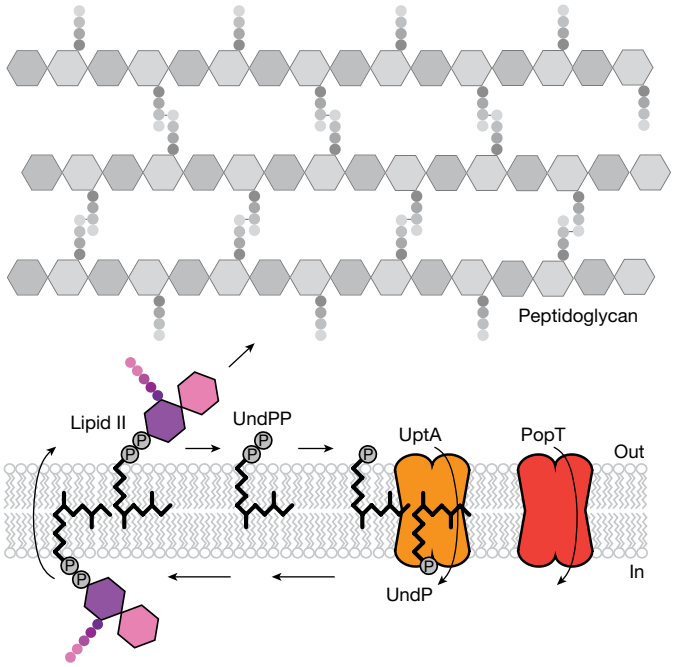

Fig. 1 | UptA and PopT complete the lipid II cycle. Schematic of the lipid II cycle in peptidoglycan synthesis highlighting the role of UptA and PopT in recycling UndP.

promoter sensitized *B. subtilis* to MX2401 (Extended Data Fig. 2h). Notably, reducing de novo synthesis of UndP sensitized *B. subtilis* to loss of *yngC* (Extended Data Fig. 3a,b), providing further support for the idea that YngC recycles the lipid carrier.

B. subtilis encodes five additional DedA paralogues. Individual deletions in these genes did not affect the MIC of MX2401 (Extended Data Fig. 3c). A deletion of one of the paralogues, *ykoX*, modestly reduced the MIC of the Δ*yngC* mutant, and a strain lacking all six paralogues phenocopied the Δ*yngC*Δ*ykoX* double mutant (Fig. 2b). Thus, YngC is likely to be the principal *B. subtilis* DedA family member involved in UndP recycling. We note that overexpression of YkoX in the Δ*yngC* mutant provided some resistance to MX2401 (Fig. 2f and Extended Data Fig. 3d). These data raise the possibility that YkoX transports a distinct anionic lipid but can act on UndP when overexpressed.

Tn-seq screens in *Staphylococcus aureus* to profile the phenotypic responsiveness to 32 antibiotics identified transposon insertions upstream of two genes (*SAOUHSC_02816* and *00846*) when the transposon library was challenged with sub-inhibitory doses of amphomycin[16] (Extended Data Fig. 4a). *02816* encodes a DedA family member, and *00846* encodes a protein with a domain of unknown function, DUF368. We validated these uncharacterized hits and found that overexpression of either protein in *S. aureus* increased the MIC of MX2401 (Fig. 2c). Deletion of *02816* did not impact the MIC of MX2401 whereas deletion of *00846* reduced it by fourfold (Fig. 2c). Strikingly, the MIC of the double mutant was about 256-fold lower than that of the wild type (Fig. 2c). Furthermore, the double mutant was growth-impaired and exhibited cell size variability, and 10% of the cells had membrane permeability defects, consistent with impaired envelope assembly (Fig. 2d,e and Extended Data Fig. 4b,c). Overexpression of either *S. aureus* gene in

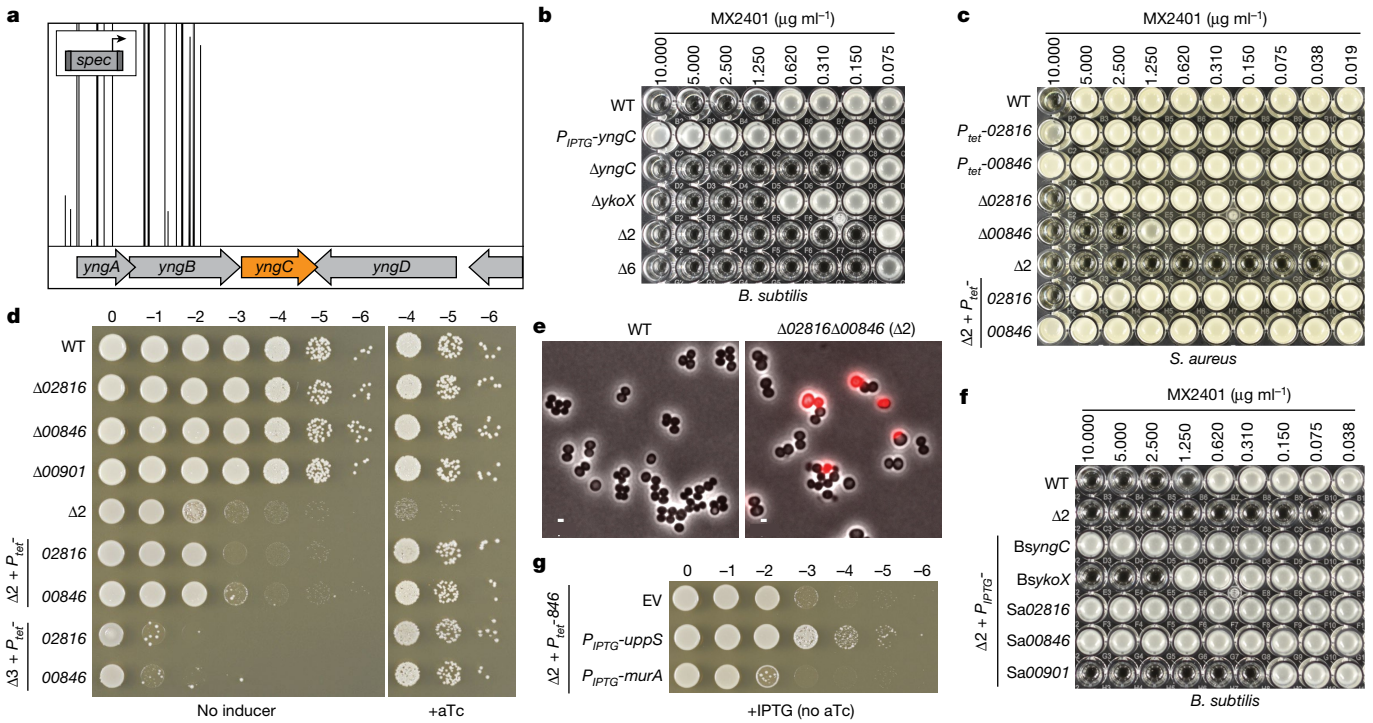

Fig. 2 | DedA and DUF368 family members provide resistance to UndP-targeting antibiotics. a, A Tn-seq screen for MX2401-resistance mutants identifies *yngC*. The transposon insertion profile at the indicated *B. subtilis* genomic region is shown. Each vertical line indicates a transposon insertion site; its height reflects the number of sequencing reads at this position. All transposons in this region were inserted with the outward-facing promoter facing *yngC* as indicated in the schematic. Most insertion sites had >20,000 reads, but the window size was scaled to 5,000 to highlight the absence of reads in the neighbouring genes. **b**, MIC assay of the indicated *B. subtilis* strains. Δ6 lacks all DedA paralogues. WT, wild type; IPTG, isopropyl-β-D-thiogalactopyranoside. **c**, MIC assay of the indicated *S. aureus* strains. **d**, Spot-dilution assays of the indicated *S. aureus* strains on tryptic soy broth agar with or without 100 ng ml^{-1} anhydrotetracycline (aTc). Δ3 lacks 02816, 00846 and 00901. **e**, Representative images of wild-type and *Δ00846Δ02816* (*Δ2*) *S. aureus* cells. Overlays of phase-contrast and propidium iodide fluorescence images are shown. Scale bars, 1 μm. **f**, MIC assays of the indicated *B. subtilis* strains overexpressing DedA and DUF368 family members from *B. subtilis* and *S. aureus*. **g**, Spot dilutions of the indicated *S. aureus* strains harbouring an empty vector (EV) or a vector with an isopropyl-β-D-thiogalactopyranoside-regulated promoter fused to *uppS* or *murA*.

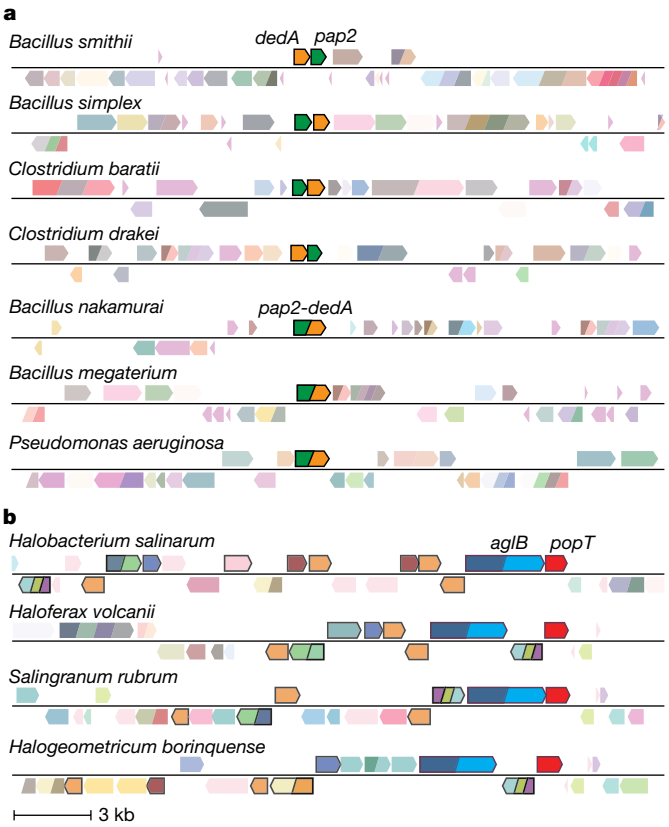

Fig. 3 | Gene neighbourhood analyses for DedA and DUF368 family members. **a**,**b**, Representative genomic neighbourhood diagrams highlight the synteny or fusion of a *dedA* gene with a gene encoding a PAP2 lipid phosphatase (**a**) and the synteny of *duf368* with genes involved in archaeal N-linked protein glycosylation pathways (**b**). About 1.3% of all *dedA* genes are fused to *pap2* genes. The gene encoding the oligosaccharyltransferase AglB is shown in blue, and other genes in the glycosylation pathway are highlighted by black borders. Thirty-seven per cent of *duf368* genes are present in gene clusters encoding protein glycosylation pathways. kb, kilobases.

B. subtilis lacking *yngC* and *ykoX* provided resistance to MX2401 (Fig. 2f). As *B. subtilis* lacks a DUF368 homologue, these data suggest that the *S. aureus* DUF368 protein functions as an UndP transporter rather than a regulator or co-factor. DUF368 is a polytopic membrane protein that is widely conserved in bacteria and archaea (Supplementary Fig. 3). The AlphaFold-predicted structure of *S. aureus* DUF368 resembles the structure of canonical membrane transporters with twofold inverted symmetry and membrane re-entrant loops on either side of the lipid bilayer[13,17] (Extended Data Fig. 2d and Supplementary Fig. 2b). The predicted gap between transmembrane helices 4 and 11 could allow the polyprenyl tail to remain in the lipid bilayer during transport of the phosphate headgroup, akin to the membrane-spanning groove in the eukaryotic TMEM16 and GPCR families[18,19] that transport lipids through the credit card mechanism[20]. On the basis of the findings presented thus far and those below, we have renamed the DedA superfamily members encoded by *yngC* and *02816* as UptA (for UndP transporter A) and the DUF368 proteins as PopT (polyprenyl-phosphate transporter).

S. aureus encodes a second DedA paralogue (*SAOUHSC_00901*) that was not identified in the Tn-seq screen described above. Overexpression of this gene in the *B. subtilis* Δ*uptA*Δ*ykoX* double mutant increased resistance to MX2401 by fourfold (Fig. 2f), suggesting that 00901 is also capable of UndP transport. Notably, the *S. aureus* triple mutant lacking *uptA*, *popT* and *00901* was not viable (Fig. 2d), consistent with the requirement for UndP recycling in cell wall biogenesis. Furthermore, overexpression of UppS, responsible for de novo synthesis of UndP but not MurA that catalyses the first committed step in peptidoglycan precursor synthesis, largely suppressed the growth defect of the *S. aureus* Δ*uptA*Δ*popT* double mutant and restored viability to the triple mutant (Fig. 2g and Extended Data Fig. 4d), providing further support for the idea that these factors recycle UndP. Finally, we determined the MICs of 12 antibiotics that target different steps in cell wall synthesis or other essential processes in wild-type *B. subtilis* and *S. aureus* and their respective mutants. Virtually all of the MICs in a *B. subtilis* Δ*uptA* mutant were indistinguishable from that of the wild type, and most MICs were 1–2-fold lower in the *S. aureus* Δ*uptA*Δ*popT* double mutant compared to that of the wild type (Supplementary Table 1). The only exception was tunicamycin, which competes with inward-facing UndP for binding to MraY[21]. The *S. aureus* double mutant was highly susceptible to this drug, consistent with reduced levels of inward-facing UndP due to an accumulation of outward-facing UndP in the mutant. Collectively, these assays argue that the functions of UptA and PopT are specific to UndP recycling.

Syntenic analyses of *uptA* and *popT*

Gene neighbourhood analysis[22] provides further support for a role of these two protein families in UndP transport. In a subset of bacterial genomes, genes encoding a DedA superfamily member and a lipid phosphatase of the PAP2 family[23] are adjacent to each other; in others the two genes are fused (Fig. 3a and Extended Data Fig. 5a–c). Some PAP2 homologues, such as *B. subtilis* BcrC and *Escherichia coli* PgpB, are UndPP phosphatases that convert surface-exposed UndPP to UndP before their transport to the cytoplasmic face of the membrane[24]. Similarly, in other bacterial genomes a gene encoding a DedA family member is present adjacent to *uppP* that encodes a second family of UndPP phosphatases[25] (Extended Data Fig. 5d,e). Accordingly, if these DedA paralogues transport UndP, then the adjacent or fused genes would encode enzymes that catalyse sequential steps in the lipid II cycle (Fig. 1). Analysis of all the *dedA* genes from two species in which one of the paralogues resides adjacent to a *pap2* or *uppP* gene is consistent with this model (Extended Data Fig. 5f,g). In the case of PopT, most archaeal genomes contain a cluster of genes required for surface protein glycosylation[26]. A DUF368-containing gene is also present in many archaeal genomes, and 37% of the time it is found in these clusters, often adjacent to an oligosaccharyltransferase of the *aglB* family (Fig. 3b and Extended Data Fig. 6a–c). The transfer of the lipid-linked oligosaccharide onto a surface protein by AglB liberates DolP that could then be recycled by the PopT homologue. Finally, Gram-positive bacteria encode enzymes involved in glycosylating surface polymers, and a DedA superfamily member is sometimes encoded in an operon with these enzymes. *B. subtilis* provides a prototypical example (Extended Data Fig. 6d). In this bacterium, a transcription factor controls the expression of two operons that are thought to be involved in glycosylation of lipoteichoic acids[27]. Four of the genes in these operons encode the full set of enzymes required to glycosylate this surface polymer. The fifth encodes UptA, which would complete the cycle in this sugar modification pathway (Extended Data Fig. 6e). Thus, gene neighbourhood analysis suggests that UptA and PopT family members are broadly conserved polyprenyl-phosphate transporters.

UptA and PopT reduce surface-exposed UndP

To directly test whether UptA and PopT family members function in UndP recycling, we conjugated a fluorescent dye to MX2401 (MX2401–FL) and used it to visualize UndP. Control experiments established that membrane labelling with MX2401–FL correlates with UndP levels (Extended Data Fig. 7a) and that the fluorescent probe cannot traverse the membrane and therefore reports on outward-facing UndP (Extended Data Fig. 7b). Wild-type *B. subtilis* cells expressing cytoplasmic blue fluorescent protein and the Δ*uptA*Δ*ykoX* double mutant expressing mCherry were mixed, labelled with MX2401–FL

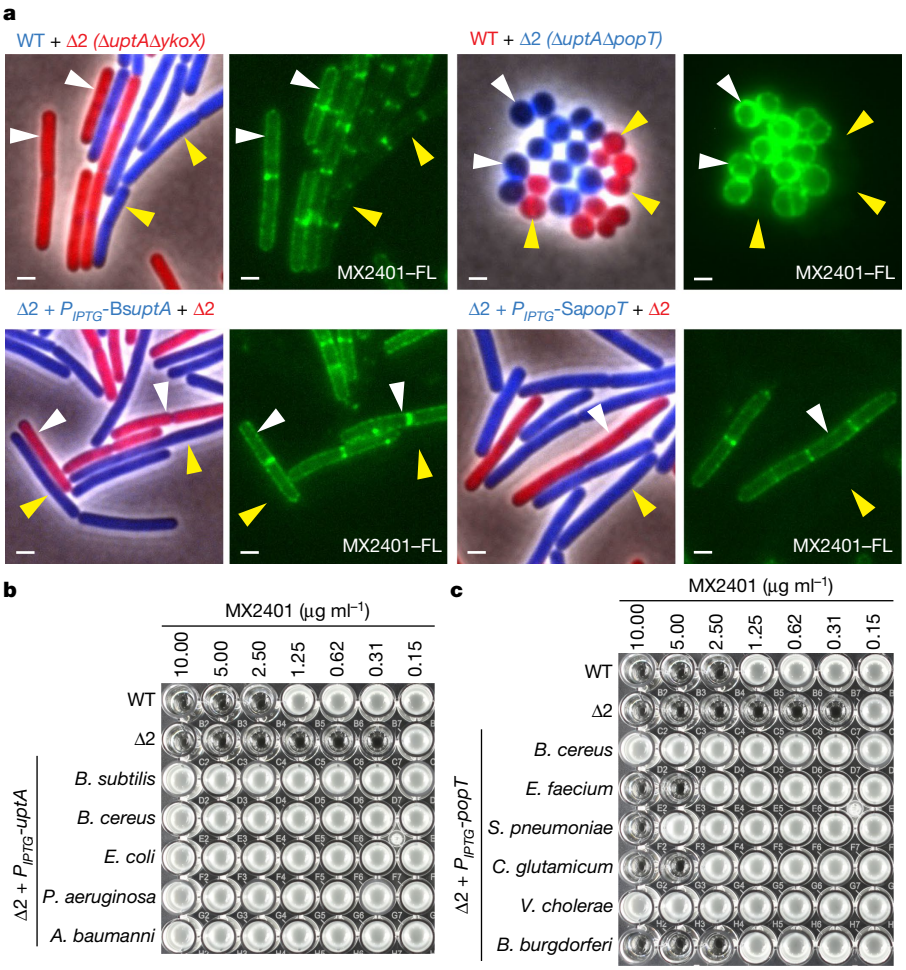

Fig. 4 | UptA and PopT are broadly conserved UndP transporters. **a**, Representative images of the indicated *B. subtilis* or *S. aureus* strains. Two strains expressing different fluorescent proteins (*B. subtilis*) or labelled with different fluorescent D-amino acids (*S. aureus*) were mixed and then stained with fluorescent MX2401 (MX2401–FL). Left, overlays of phase-contrast and fluorescence images in the red and blue channels to distinguish the two strains. Right, MX2401–FL staining. Yellow arrowheads highlight wild-type cells or cells overexpressing *Bs*UptA or *Sa*PopT. White arrowheads highlight cells lacking the UndP transporters. Scale bars, 1 μm. **b**,**c**, MIC assays of *B. subtilis* strains overexpressing UptA (**b**) or PopT (**c**) homologues from the indicated bacteria. *E. faecium*, *Enterococcus faecium*.

and visualized by fluorescence microscopy. Wild-type cells had a faint MX2401–FL signal along the cytoplasmic membrane whereas cells lacking the two DedA paralogues had an approximately twofold higher level of membrane fluorescence (Fig. 4a and Extended Data Figs. 7c and 8a,b). Notably, the MX2401–FL signal in the *B. subtilis* double mutant was markedly reduced when *Bs*UptA, *Sa*UptA or *Sa*PopT was overexpressed (Fig. 4a and Extended Data Fig. 7c). In an analogous experiment, we labelled wild-type *S. aureus* and the Δ*uptA*Δ*popT* double mutant with spectrally distinct fluorescent D-amino acids[28] and then mixed the two cultures and stained them with MX2401–FL. The double mutant had strong MX2401–FL fluorescence whereas the signal was barely detectable in the wild type (Fig. 4a and Extended Data Fig. 7c). Similar results were obtained when MX2401 was labelled with three other fluorescent dyes including Alex Fluor 488, which prevents membrane permeation of its conjugates[29–31] (Extended Data Fig. 9a–c).

E. coli encodes eight DedA superfamily members[8]. The mutants have pleiotropic phenotypes that include defects in cell division, morphology, alkaline tolerance, membrane potential and antibiotic resistance[8,32–34]. The proteins have been proposed to function as proton-dependent transporters that help maintain the proton motive force[8,35]. We note that the proton motive force was intact in the *B. subtilis* Δ*uptA*Δ*ykoX* and *S. aureus* Δ*uptA*Δ*popT* double mutants (Extended Data Fig. 10). To investigate whether any of the *E. coli* DedA paralogues catalyse UndP transport, we expressed each in *B. subtilis* and tested for MX2401 resistance. Although several increased the MIC of MX2401 of the *B. subtilis* Δ*uptA*Δ*ykoX* mutant by about 2–4-fold, only one conferred high-level resistance (Fig. 4b and Extended Data Fig. 9d). This DedA paralogue (DedA) is the founding member of the superfamily and is most similar to *Bs*UptA and *Sa*UptA (Supplementary Fig. 2a and Supplementary Table 2a). We extended this cross-species complementation analysis to a diverse collection of UptA and PopT homologues. The DedA superfamily members tested were chosen on the basis of their similarity to the validated UptA family members. In addition to *Sa*UptA and *Ec*UptA, homologues from *Acinetobacter baumannii*, *Pseudomonas aeruginosa* and *Bacillus cereus* conferred MX2401 resistance to the *B. subtilis* double mutant (Fig. 4b). Similarly, expression of PopT homologues from *B. cereus*, *Streptococcus pneumoniae*, *Vibrio cholerae*, *Borrelia burgdorferi* and *Corynebacterium glutamicum* increased the MIC of MX2401 (Fig. 4c). Notably, all five of the proteins tested also reduced the level of surface-exposed UndP as assayed by MX2401–FL (Extended Data Fig. 8c,d).

Conclusions

We conclude that UptA and PopT family members catalyse the transport of UndP, the final step in virtually all cell envelope biogenesis and surface

modification pathways in both Gram-positive and Gram-negative bacteria. Their discovery completes the parts list for many of these intensively studied pathways and represents a new set of targets to potentiate the current arsenal of antibiotics.

The mechanisms of UndP transport by UptA and PopT are unknown at present. Recent in vitro reconstitution experiments of two eukaryotic DedA superfamily members, TMEM41B and VMP1 (ref. [36]), were found to redistribute fluorescently labelled phospholipids with diverse headgroups from the luminal to the exposed face of proteoliposomes. Lipid transport was energy independent, suggesting that these transporters function as lipid scramblases. Our work has uncovered a role for UptA and PopT in retrograde transport of UndP, but we cannot exclude a model in which UptA or PopT act as scramblases. If our conclusions are correct, the transfer of sugars onto the lipid carrier on the cytoplasmic face of the membrane would result in concentration-driven retrograde transport. Future work will focus on characterizing the mechanism of UndP transport of UptA and PopT in vitro. Notably, depletion of either TMEM41B or VMP1 in tissue culture cells led to defects in the sorting of cholesterol, phosphatidylserine and phosphatidylcholine, suggesting that these proteins function in lipid transport in vivo[36,37]. The analysis of UptA family members presented here strengthens this conclusion and suggests that other bacterial DedA superfamily members function in lipid transport. On the basis of our analysis of the *B. subtilis* DedA paralogues, we reason that in vivo these transporters have more narrow substrate specificity and act on distinct lipids. Furthermore, it is tempting to speculate that a DedA superfamily member recycles DolP in eukaryotes whereas PopT homologues transport DolP in archaea.

Other than an increase in surface-exposed UndP, the *B. subtilis* Δ*uptA*Δ*ykoX* double mutant had no discernible growth or morphological defects whereas the *S. aureus* Δ*uptA*Δ*popT* double mutant was growth-impaired and the triple mutant was inviable. These data raise the possibility that *B. subtilis* encodes a third family of UndP transporters or that UndP flipping can occur spontaneously albeit inefficiently. We favour the latter model because a screen using a transposon with an even stronger outward-facing promoter did not identify additional hits when the *B. subtilis* Δ*uptA*Δ*ykoX* double mutant was challenged with MX2401. Furthermore, no genes were identified as synthetic lethal with the single or double *B. subtilis* mutants. UppP has been proposed to function as both an UndPP phosphatase and an UndP transporter[3,38], but overexpression or deletion of *uppP* or *bcrC* in *B. subtilis* had no impact on the MIC of MX2401 (Extended Data Fig. 9e) and neither gene was identified as a hit in our Tn-seq screen nor the one carried out in *S. aureus* (Extended Data Fig. 4a). These observations lead us to suggest that UndP can spontaneously flip-flop in the cytoplasmic membrane and that the extent of protonation of the phosphate headgroup influences efficiency. Transmembrane pH gradients have been shown to cause asymmetric distribution of phosphatidic acid within artificial bilayers[39], and the pH gradient maintained by the proton motive force could similarly lead to an asymmetry of UndP. This model could also explain why the Δ*popT*Δ*uptA* synthetic lethality observed in *V. cholerae* was suppressed in acidic conditions[40]. However, at this stage we cannot rule the possibility that additional families of transporters contribute to UndP recycling and will continue screening for these factors in the future.

Although not essential, the DedA superfamily member that is most similar to *E. coli* DedA (*Ec*UptA) in *Neisseria meningitidis, Klebsiella pneumoniae* and *Burkholderia thailandensis* (Supplementary Table 2b) is required for intrinsic resistance to the last-resort antibiotic colistin[35,41,42]. Loss-of-function mutations in the associated genes in these Gram-negative pathogens confer colistin sensitivity, and in some cases it has been shown that expression of *Ec*UptA can reverse this sensitivity, implicating UndP transport. Colistin resistance is mediated by aminoarabinose modification to lipid A of lipopolysaccharide, which reduces its affinity for polycationic antibiotics[43]. The aminoarabinose modification is built on UndP in the cytoplasm, flipped to the periplasm and then transferred to lipid A. Alterations in these DedA superfamily members result in low levels of aminoarabinose-modified lipid A[35], and we reason that the reduction in UndP recycling in these mutants accounts for the decreased modification. UptA homologues in *K. pneumoniae* and *A. baumannii* are also required for resistance to complement-mediated killing and *K. pneumoniae* UptA is additionally required for neutrophil evasion in a mouse model for lung colonization[44–46]. Long O-antigen chains and a thick capsule, both glycopolymers that are built on UndP, are primary defence mechanisms of these pathogens. Thus, small molecules that target UptA and PopT transporters could potentiate both last-resort antibiotics and host-defence-mediated killing.

Online content

Any methods, additional references, Nature Portfolio reporting summaries, source data, extended data, supplementary information, acknowledgements, peer review information; details of author contributions and competing interests; and statements of data and code availability are available at https://doi.org/10.1038/s41586-022-05587-z.

1. Rush, J. S., Gao, N., Lehrman, M. A. & Waechter, C. J. Recycling of dolichyl monophosphate to the cytoplasmic leaflet of the endoplasmic reticulum after the cleavage of dolichyl pyrophosphate on the lumenal monolayer. *J. Biol. Chem.* **283**, 4087–4093 (2008).
2. Eichler, J. & Guan, Z. Lipid sugar carriers at the extremes: the phosphodolichols Archaea use in N-glycosylation. *Biochim. Biophys. Acta* **1862**, 589–599 (2017).
3. Workman, S. D. & Strynadka, N. C. J. A Slippery scaffold: synthesis and recycling of the bacterial cell wall carrier lipid. *J. Mol. Biol.* **432**, 4964–4982 (2020).
4. Manat, G. et al. Deciphering the metabolism of undecaprenyl-phosphate: the bacterial cell-wall unit carrier at the membrane frontier. *Microb. Drug Resist.* **20**, 199–214 (2014).
5. Tanaka, H., Ôiwa, R., Matusukura, S. & Ômura, S. Amphomycin inhibits phospho-*N*-acetylmuramyl-pentapeptide translocase in peptidoglycan synthesis of *Bacillus*. *Biochem. Biophys. Res. Commun.* **86**, 902–908 (1979).
6. Rubinchik, E. et al. Mechanism of action and limited cross-resistance of new lipopeptide MX-2401. *Antimicrob. Agents Chemother.* **55**, 2743–2754 (2011).
7. Singh, M., Chang, J., Coffman, L. & Kim, S. J. Solid-state NMR characterization of amphomycin effects on peptidoglycan and wall teichoic acid biosyntheses in *Staphylococcus aureus*. *Sci. Rep.* **6**, 31757 (2016).
8. Doerrler, W. T., Sikdar, R., Kumar, S. & Boughner, L. A. New functions for the ancient DedA membrane protein family. *J. Bacteriol.* **195**, 3–11 (2013).
9. Typas, A., Banzhaf, M., Gross, C. A. & Vollmer, W. From the regulation of peptidoglycan synthesis to bacterial growth and morphology. *Nat. Rev. Microbiol.* **10**, 123–136 (2012).
10. Piepenbreier, H., Diehl, A. & Fritz, G. Minimal exposure of lipid II cycle intermediates triggers cell wall antibiotic resistance. *Nat. Commun.* **10**, 2733 (2019).
11. Barreteau, H. et al. Quantitative high-performance liquid chromatography analysis of the pool levels of undecaprenyl phosphate and its derivatives in bacterial membranes. *J. Chromatogr. B* **877**, 213–220 (2009).
12. Dobihal, G. S., Flores-Kim, J., Roney, I. J., Wang, X. & Rudner, D. Z. The WalR-WalK signaling pathway modulates the activities of both CwlO and LytE through control of the peptidoglycan deacetylase PdaC in *Bacillus subtilis*. *J. Bacteriol.* https://doi.org/10.1128/jb.00533-21 (2021).
13. Viklund, H., Granseth, E. & Elofsson, A. Structural classification and prediction of reentrant regions in α-helical transmembrane proteins: application to complete genomes. *J. Mol. Biol.* **361**, 591–603 (2006).
14. Eiamphungporn, W. & Helmann, J. D. The *Bacillus subtilis* σM regulon and its contribution to cell envelope stress responses. *Mol. Microbiol.* **67**, 830–848 (2008).
15. Helmann, J. D. *Bacillus subtilis* extracytoplasmic function (ECF) sigma factors and defense of the cell envelope. *Curr. Opin. Microbiol.* **30**, 122–132 (2016).
16. Santiago, M. et al. Genome-wide mutant profiling predicts the mechanism of a lipid II binding antibiotic. *Nat. Chem. Biol.* **14**, 601–608 (2018).
17. Forrest, L. R. Structural symmetry in membrane proteins. *Biophysics* **44**, 311–337 (2015).
18. Brunner, J. D., Lim, N. K., Schenck, S., Duerst, A. & Dutzler, R. X-ray structure of a calcium-activated TMEM16 lipid scramblase. *Nature* **516**, 207–212 (2014).
19. Morra, G. et al. Mechanisms of lipid scrambling by the G protein-coupled receptor opsin. *Structure* **26**, 356–367 (2018).
20. Pomorski, T. & Menon, A. K. Lipid flippases and their biological functions. *Cell. Mol. Life Sci.* **63**, 2908–2921 (2006).
21. Muramatsu, Y., Ishii, M. M. & Inukai, M. Studies on novel bacterial translocase I inhibitors, A-500359s. *J. Antibiotics* **56**, 253–258 (2003).
22. Zallot, R., Oberg, N. & Gerlt, J. A. The EFI web resource for genomic enzymology tools: leveraging protein, genome, and metagenome databases to discover novel enzymes and metabolic pathways. *Biochemistry* **58**, 4169–4182 (2019).
23. Brindley, D. N. & Waggoner, D. W. Mammalian lipid phosphate phosphohydrolases. *J. Biol. Chem.* **273**, 24281–24284 (1998).
24. Ghachi, M. E., Derbise, A., Bouhss, A. & Mengin-Lecreulx, D. Identification of multiple genes encoding membrane proteins with undecaprenyl pyrophosphate phosphatase (UppP) activity in *Escherichia coli*. *J. Biol. Chem.* **280**, 18689–18695 (2005).

25. Ghachi, M. E., Bouhss, A., Blanot, D. & Mengin-Lecreulx, D. The *bacA* gene of *Escherichia coli* encodes an undecaprenyl pyrophosphate phosphatase activity. *J. Biol. Chem.* **279**, 30106–30113 (2004).
26. Jarrell, K. F. et al. N-linked glycosylation in *Archaea*: a structural, functional, and genetic analysis. *Microbiol. Mol. Biol. R* **78**, 304–341 (2014).
27. Wu, C.-H. et al. *Bacillus subtilis* YngB contributes to wall teichoic acid glucosylation and glycolipid formation during anaerobic growth. *J. Biol. Chem.* **296**, 100384 (2021).
28. Kuru, E., Tekkam, S., Hall, E., Brun, Y. V. & Nieuwenhze, M. S. V. Synthesis of fluorescent D-amino acids and their use for probing peptidoglycan synthesis and bacterial growth in situ. *Nat. Protoc.* **10**, 33–52 (2015).
29. Panchuk-Voloshina, N. et al. Alexa dyes, a series of new fluorescent dyes that yield exceptionally bright, photostable conjugates. *J. Histochem. Cytochem.* **47**, 1179–1188 (1999).
30. Hapuarachchige, S. et al. Design and synthesis of a new class of membrane-permeable triazaborolopyridinium fluorescent probes. *J. Am. Chem. Soc.* **133**, 6780–6790 (2011).
31. Grimm, J. B. et al. A general method to improve fluorophores for live-cell and single-molecule microscopy. *Nat. Methods* **12**, 244–250 (2015).
32. Sikdar, R. & Doerrler, W. T. Inefficient Tat-dependent export of periplasmic amidases in an *Escherichia coli* strain with mutations in two DedA family genes. *J. Bacteriol.* **192**, 807–818 (2010).
33. Kumar, S. & Doerrler, W. T. Members of the conserved DedA family are likely membrane transporters and are required for drug resistance in *Escherichia coli*. *Antimicrob. Agents Chemother.* **58**, 923–930 (2014).
34. Boughner, L. A. & Doerrler, W. T. Multiple deletions reveal the essentiality of the DedA membrane protein family in *Escherichia coli*. *Microbiology* **158**, 1162–1171 (2012).
35. Panta, P. R. & Doerrler, W. T. A *Burkholderia thailandensis* DedA family membrane protein is required for proton motive force dependent lipid A modification. *Front. Microbiol.* **11**, 618389 (2021).
36. Li, Y. E. et al. TMEM41B and VMP1 are scramblases and regulate the distribution of cholesterol and phosphatidylserine. *J. Cell Biol.* **220**, e202103105 (2021).
37. Huang, D. et al. TMEM41B acts as an ER scramblase required for lipoprotein biogenesis and lipid homeostasis. *Cell Metab.* **33**, 1655–1670 (2021).
38. Ghachi, M. E. et al. Crystal structure of undecaprenyl-pyrophosphate phosphatase and its role in peptidoglycan biosynthesis. *Nat. Commun.* **9**, 1078 (2018).
39. Eastman, S. J., Hope, M. J. & Cullis, P. R. Transbilayer transport of phosphatidic acid in response to transmembrane pH gradients. *Biochemistry* **30**, 1740–1745 (1991).
40. Sit, B. et al. Undecaprenyl phosphate translocases confer conditional microbial fitness. *Nature* https://doi.org/10.1038/s41586-022-05569-1 (2022).
41. Tzeng, Y.-L. et al. Cationic antimicrobial peptide resistance in *Neisseria meningitidis*. *J. Bacteriol.* **187**, 5387–5396 (2005).
42. Tiwari, V. et al. A *Klebsiella pneumoniae* DedA family membrane protein is required for colistin resistance and for virulence in wax moth larvae. *Sci. Rep.* **11**, 24365 (2021).
43. Moskowitz, S. M., Ernst, R. K. & Miller, S. I. PmrAB, a two-component regulatory system of *Pseudomonas aeruginosa* that modulates resistance to cationic antimicrobial peptides and addition of aminoarabinose to lipid A. *J. Bacteriol.* **186**, 575–579 (2004).
44. Short, F. L. et al. Genomic profiling reveals distinct routes to complement resistance in *Klebsiella pneumoniae*. *Infect. Immun.* **88**, e00043-20 (2020).
45. Paczosa, M. K. et al. Transposon mutagenesis screen of *Klebsiella pneumoniae* identifies multiple genes important for resisting antimicrobial activities of neutrophils in mice. *Infect. Immun.* **88**, e00034-20 (2020).
46. Sanchez-Larrayoz, A. F. et al. Complexity of complement resistance factors expressed by *Acinetobacter baumannii* needed for survival in human serum. *J. Immunol.* **199**, 2803–2814 (2017).

Methods

General methods

All *B. subtilis* strains were derived from the prototrophic strain PY79 (ref. [47]). All *B. subtilis* experiments were carried out at 37 °C with aeration in lysogeny broth (LB). Antibiotic concentrations used were: 100 μg ml^{-1} spectinomycin, 10 μg ml^{-1} kanamycin, 5 μg ml^{-1} chloramphenicol, 10 μg ml^{-1} tetracycline, 1 μg ml^{-1} erythromycin and 25 μg ml^{-1} lincomycin (MLS). Isopropyl-β-D-thiogalactopyranoside (IPTG) was used at a concentration of 500 μM unless indicated otherwise. All experiments with MX2401 or amphomycin used medium supplemented with 25 μg ml^{-1} $CaCl_2$. All *B. subtilis* strains were generated using the one-step competence method unless indicated otherwise. All *S. aureus* strains were derived from RN4220. Cells were grown at 37 °C with aeration in tryptic soy broth. Antibiotic concentrations used were: 7.5 μg ml^{-1} erythromycin, 50 μg ml^{-1} kanamycin, 450 μg ml^{-1} spectinomycin, 5 μg ml^{-1} chloramphenicol. Anhydrotetracycline was used at a concentration of 100 ng ml^{-1} unless indicated otherwise. Transductions were carried out using phage 80α. All strains, plasmids, oligonucleotides and synthetic DNA used in this study can be found in Supplementary Tables 3–6.

Statistics and reproducibility

All MIC experiments were carried out in at least biological triplicate and representative images are shown. All microscopy analyses were carried out in at least biological duplicate with many fields of view analysed and representative images are shown. Spot assays and streak analysis were carried out in at least biological triplicate. Western blotting was carried out in biological duplicate. Attempts at replication for all experiments were successful.

Transposon mutagenesis and suppressor isolation

Transposon libraries were generated as described previously[12]; libraries were generated using pIR242, an *E. coli–B. subtilis* shuttle vector containing a temperature-sensitive replicon for *B. subtilis*, the mariner-Himar1 transposase, and a spectinomycin resistance cassette followed by a strong outward-facing promoter (*Ppen*) and flanked by inverted repeats recognized by the transposase. The pIR242 plasmid was separately transformed into BIR769 or BIR672 and plated on LB agar supplemented with MLS and incubated at 30 °C. Transformants were inoculated into LB supplemented with spectinomycin and grown with aeration at 22 °C for 24 h. Cultures were pooled and frozen with 15% glycerol. Aliquots of the frozen stocks were thawed and plated onto LB agar supplemented with spectinomycin, $CaCl_2$ and 2.5 μg ml^{-1} MX2401 (BIR769) or 0.3 μg ml^{-1} MX2401 (BIR672). Plates were incubated at 42 °C overnight to select for transposon-mutagenized cells that had lost the plasmid and acquired resistance to MX2401.

Mapping transposon insertion sites

Sequencing and mapping of the transposon insertion sites was carried out as described previously[12,48]. In brief, transposon-mutagenized colonies that grew on LB agar supplemented with MX2401 were pooled, and genomic DNA was extracted. DNA was digested with MmeI and ligated to adaptors. Transposon–chromosome junctions were amplified by PCR, and the products were size selected using a 2% agarose gel. The Illumina MiSeq platform was used to sequence the library. Sequencing reads were mapped to the *B. subtilis* 168 chromosome (NCBI NC_00964.3) using Bowtie 1.0.0. All next-generation sequencing datasets generated in this work have been deposited to the NCBI Sequence Read Archive within project PRJNA898639 (SAMN31619234 and SAMN31619233). Reanalysis of Tn-seq data from an earlier study[16] was carried out as described in the methods of that publication using sequences previously deposited on the NCBI Sequence Read Archive (SRX3390726).

MIC assays

Exponentially growing cultures of *B. subtilis* or *S. aureus* were back-diluted 1:1,000 into 96-well microtitre plates containing the indicated concentrations of antibiotic and inducers. Plates were sealed with breathable membranes and the cultures were grown with orbital shaking at 37 °C overnight. Plates were photographed after the overnight (about 16 h) incubation.

Spot-dilution assays

Late-log cultures were normalized to optical density at 600 nm (OD_{600nm}) = 1, and tenfold serial dilutions were generated. A 5 μl volume of each dilution was spotted onto LB agar supplemented with or without IPTG or onto tryptic soy broth agar supplemented with or without anhydrotetracycline, IPTG or 3 μg ml^{-1} fosfomycin. Plates were incubated at 37 °C overnight and photographed the next day.

Genomic neighbourhood analysis

The Enzyme Similarity Tool (EFI-EST v2.0) from the Enzyme Function Initiative[22] (available at https://efi.igb.illinois.edu/efi-est/) was used to generate sequence similarity networks for the DedA and DUF368 protein families from the pfam entries SNARE_assoc (PF09335) and DUF368 (PF04018), respectively. Owing to the large size of the SNARE_assoc family, the UniRef90 database was used. The sequence similarity networks were then used as inputs for carrying out genomic neighbourhood analysis using the Enzyme Function Initiative Genome Neighborhood Tool[22] (EFI-GNT v1.0) available at https://efi.igb.illinois.edu//efi-gnt/index.php. Alignment score cutoffs of 35% were used for both analyses. Gene neighbourhood diagrams were generated to visualize the 10 nearest genes surrounding all *dedA* and *duf368* members. A sequence similarity network was also generated for the subset of DUF368 members in archaea, this dataset was used as an input for carrying out gene neighbourhood analysis and the resulting gene neighbourhood networks were uploaded and visualized in Cytoscape. Cytoscape 3.8.2 was used to examine and quantify the genes most found within a 10-gene window of *duf368*.

MX2401–FL

MX2401 has a single primary amine[7], and drug optimization efforts have found that it can be modified without loss of potency. MX2401 was labelled at this position with three dyes reported to be membrane impermeable, CF488A, CF405M and CF594, using the Mix-n-Stain CF Dye Small Ligand Labeling Kit (Biotium, numbers 92350, 92362 and 92352) following the manufacturer's instructions. In brief, 10 μl (0.1 μmol) of MX2401 dissolved in dimethylsulfoxide (DMSO) was mixed with 2 μl of reaction buffer. The mixtures were added to individual dyes and briefly vortexed. The reactions were incubated for 30 min in the dark at room temperature. A 2 μl volume of quenching buffer was added to the reactions, briefly vortexed and incubated for 5 min in the dark. DMSO was added to a final volume of 100 μl generating 1 mM solutions of MX2401–CF488A, MX2401–CF405M and MX2401–CF594. MX2401 was labelled with Alex Fluor 488 using Alexa Fluor 488 TFP ester kit (ThermoFisher catalogue number A37570) following the manufacturer's instructions with minor modifications. In brief, 100 μg of Alexa Fluor 488 TFP ester was dissolved in 10 μl DMSO and added to 1 mg of MX2401 dissolved in 100 μl of 0.1 M HEPES pH 8.2. The mixture was incubated with shaking for 1 h in the dark at room temperature. To quench the reaction, 10 μl of 1 M Tris pH 7 was added to the reaction and was incubated with shaking for one further hour in the dark at room temperature.

MX2401–FL labelling and fluorescence microscopy

Exponentially growing cultures of *S. aureus* were incubated for 20 min with the fluorescent D-amino acids HADA (Tocris) or RADA (Tocris) at final concentrations of 100 μM. Exponentially growing cultures of

S. aureus labelled with fluorescent D-amino acids and *B. subtilis* were collected by centrifugation at 7,000 r.p.m. for 2 min. Cells were washed once with 1× PBS (pH 7.4) and resuspended in 1/25 volume of 1× PBS. MX2401–FL was added to a final concentration of 25 μM and incubated for 30 s. Cells were washed with 1× PBS, resuspended in 1/25 volume of 1× PBS and spotted onto 1.5% agarose pads containing growth medium. Propidium iodide, TMA-DPH and FM4-64 labelling procedures were carried out in 1× PBS at final concentrations of 5 μM.

Phase and fluorescence microscopy was carried out with a Nikon Ti inverted microscope using a Plan Apo 100×, 1.4 Oil Ph3 DM objective, a Lumencore SpectraX LED illumination system and an Andor Zyla 4.2 Plus sCMOS camera. Chroma ET filter cubes (numbers 49000, 49002, 49003 and 49008) were used for imaging blue fluorescent protein (BFP), HADA and TMA-DPH; MX2401–FL; YFP; and mCherry, RADA, propidium iodide and FM4-64, respectively. Exposure time of 50 ms was used for HADA, RADA, propidium iodide and mCherry; 400 ms was used for BFP; 200 ms was used for MX2401–FL, FM4-64 and TMA-DPH; and 1 s was used for YFP. Images were acquired with Nikon elements 4.3 software and analysed using ImageJ (version 2.3).

Fluorescence microscopy quantification

ImageJ was used to quantify fluorescent intensities. For quantification of YFP produced under the control of the PyngC promoter, a vegetatively expressed BFP was used to identify cell boundaries. Intensity values from the YFP channel were extracted and the background autofluorescence from an empty field of view was subtracted from the image. For quantification of MX2401–FL labelling, cells were co-stained with MX2401–FL and FM4-64. FM4-64 was used to identify cell membranes. Single-pixel-wide lines were drawn down the sidewalls of cells, avoiding overlapping cells and double membranes at septa. Average intensity values for each sidewall were extracted from the MX2401–FL channel. Background autofluorescence was taken as an average from five places in each field of view and subtracted from each intensity measurement. GraphPad Prism 9 was used for plotting.

Structural model visualization

AlphaFold2 predictions of PopT (SAOUHSC_00846) and UptA (YNGC_BACSU) were downloaded from the AlphaFold Protein Structure Database (available at https://alphafold.ebi.ac.uk/). ChimeraX1.3 was used to visualize the structural models and generate images. Re-entrant helices are highlighted in blue and red. Arginine residues critical for YngC (*Bs*UptA) function are shown as sticks.

Immunoblot analysis

Immunoblot analysis was carried out as described previously[49]. In brief, a 1-ml volume of exponentially growing cells was normalized by OD_{600nm}, and the cells were collected by centrifugation (2 min at 7,000 r.p.m.). The cell pellet was resuspended in lysis buffer (20 mM Tris pH 7.0, 10 mM $MgCl_2$, 1mM EDTA, 1 mg ml^{-1} lysozyme, 10 μg ml^{-1} DNase I, 100 μg ml^{-1} RNase A, 1 mM phenylmethylsulfonyl fluoride, 1 μg ml^{-1} leupeptin, 1 μg ml^{-1} pepstatin) and incubated at 37 °C for 15 min. An equal volume of sample buffer (0.25 M Tris pH 6.8, 4% SDS, 20% glycerol, 10 mM EDTA, 10% β-mercaptoethanol) was added to the lysis reactions and vortexed briefly to complete lysis. Proteins were separated by SDS–PAGE on 12.5% polyacrylamide gels, transferred onto Immobilon-P membranes (Millipore) by electrophoretic transfer and blocked with 5% milk in phosphate-buffered saline with 0.5% Tween-20 (PBS-T). The blocked membranes were probed with monoclonal anti-His (1:4,000; Genscript) or polyclonal anti-SigA (1:10,000)[50] antibodies diluted into 3% BSA in PBS-T. Primary antibodies were detected using horseradish-peroxidase-conjugated goat anti-rabbit IgG (1:3,000; BioRad) or goat anti-mouse IgG (1:20,000; BioRad) and the Super Signal chemiluminescence reagent as described by the manufacturer (Pierce).

Dendrograms

Dendrograms were created using AnnoTree version 1 (ref. [51]). All entries of PF04018 (DUF368) were mapped to representative dendrograms of bacteria and archaea. Hits are shown as blue lines.

Multiple sequence alignment

Multiple sequence alignments were carried out using Clustal Omega version 1.2.4 (ref. [52]) and visualized with Espript 3.0 (ref. [53]).

Reporting summary

Further information on research design is available in the Nature Portfolio Reporting Summary linked to this article.

Data availability

Next-generation sequencing datasets generated in this study have been uploaded to the NCBI Sequence Read Archive within project PRJNA898639 (SAMN31619234 and SAMN31619233). Reads were mapped to the *B. subtilis* genome (NCBI NC_00964.3). Next-generation sequencing datasets that were reanalysed from ref. [16] are available on the NCBI Sequence Read Archive (SRX3390726), and the analysis was conducted as described in the paper. Uniprot accession codes for gene neighbourhood analysis are provided in Supplementary Table 3. Details of the strains, plasmids, oligonucleotides and synthetic DNA constructs used are provided in Supplementary Tables 4–7. Source data are provided with this paper.

47. Youngman, P., Perkins, J. B. & Losick, R. Construction of a cloning site near one end of Tn917 into which foreign DNA may be inserted without affecting transposition in *Bacillus subtilis* or expression of the transposon-borne *erm* gene. *Plasmid* **12**, 1–9 (1984).
48. Meeske, A. J. et al. MurJ and a novel lipid II flippase are required for cell wall biogenesis in *Bacillus subtilis*. *Proc. Natl Acad. Sci. USA* **112**, 6437–6442 (2015).
49. Wang, X. et al. Condensin promotes the juxtaposition of DNA flanking its loading site in *Bacillus subtilis*. *Genes Dev.* **29**, 1661–1675 (2015).
50. Fujita, M. & Sadaie, Y. Rapid isolation of RNA polymerase from sporulating cells of *Bacillus subtilis*. *Gene* **221**, 185–190 (1998).
51. Mendler, K. et al. AnnoTree: visualization and exploration of a functionally annotated microbial tree of life. *Nucleic Acids Res.* **47**, 4442–4448 (2019).
52. Sievers, F. et al. Fast, scalable generation of high-quality protein multiple sequence alignments using Clustal Omega. *Mol. Syst. Biol.* **7**, 539–539 (2011).
53. Robert, X. & Gouet, P. Deciphering key features in protein structures with the new ENDscript server. *Nucleic Acids Res.* **42**, W320–W324 (2014).
54. Ogura, M., Tsukahara, K. & Tanaka, T. Identification of the sequences recognized by the *Bacillus subtilis* response regulator YclJ. *Arch. Microbiol.* **192**, 569–580 (2010).

Acknowledgements We thank all members of the Bernhardt–Rudner super-group for helpful advice, discussions and encouragement, T. Bernhardt, S. Walker and A. Kruse for insights and advice, S. Farmer and B. Hancock for MX2401, the MicRoN core for advice on microscopy, and M. Waldor for coordinating submission. Support for this work comes from the National Institute of Health grants GM086466, GM127399, GM145299 and U19 AI158028 (D.Z.R.).

Author contributions I.J.R. and D.Z.R. conceived of the study and I.J.R. carried out all experiments and analysis. D.Z.R. supervised the study. I.J.R. and D.Z.R. wrote the paper.

Competing interests The authors declare no competing interests.

Additional information

Supplementary information The online version contains supplementary material available at https://doi.org/10.1038/s41586-022-05587-z.

Correspondence and requests for materials should be addressed to David Z. Rudner.

Peer review information *Nature* thanks Carol Gross, Anant Menon and the other, anonymous, reviewer(s) for their contribution to the peer review of this work. Peer reviewer reports are available.

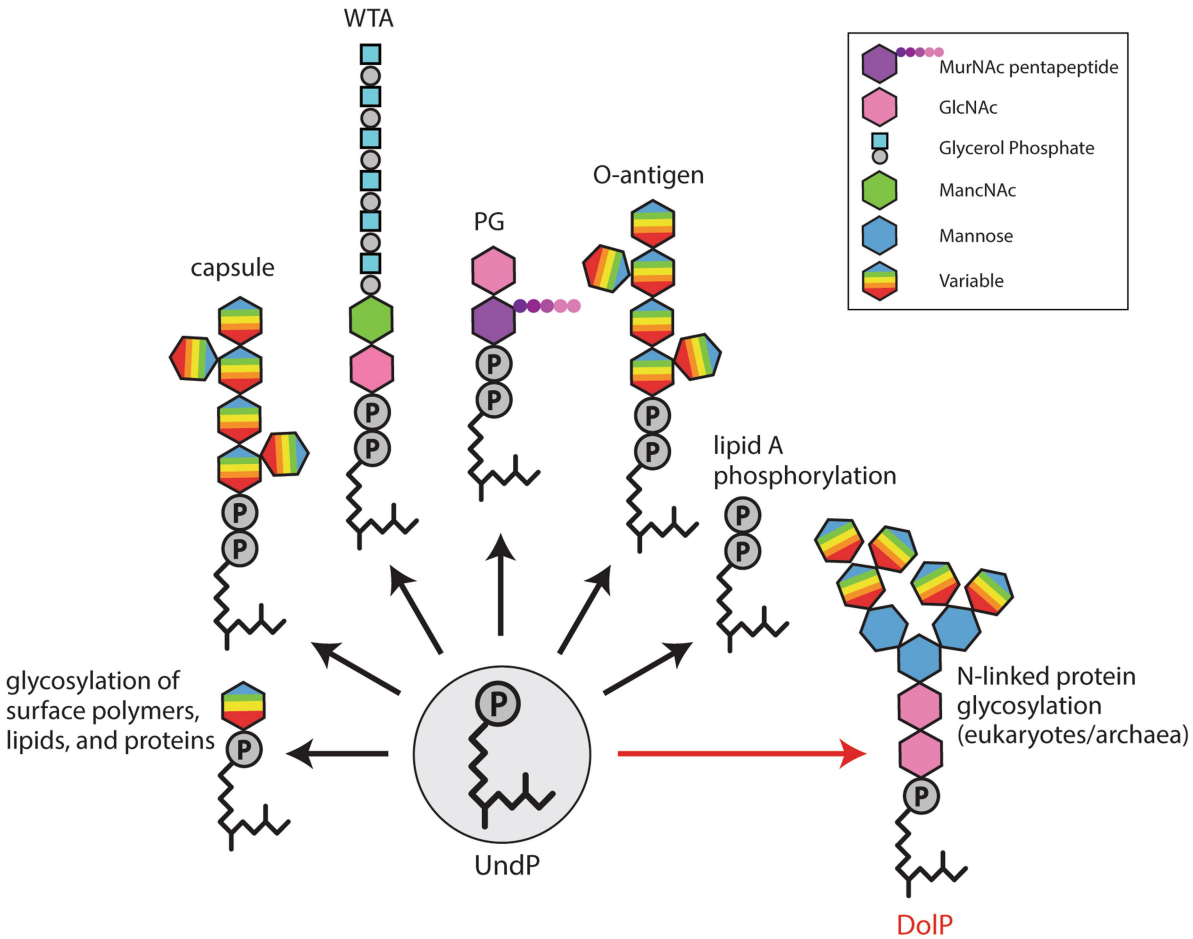

Extended Data Fig. 1 | Polyprenyl-phosphate lipids are universal transporters of surface glycopolymers. Schematic illustrating the glycopolymers and sugar modifications that are assembled on undecaprenyl-phosphate (UndP) in bacteria and on dolichol-phosphate (DolP) in archaea and eukaryotes. Although an oligosaccharide carried on DolP is shown, some eukaryotes use the pyrophosphate carrier (DolPP).

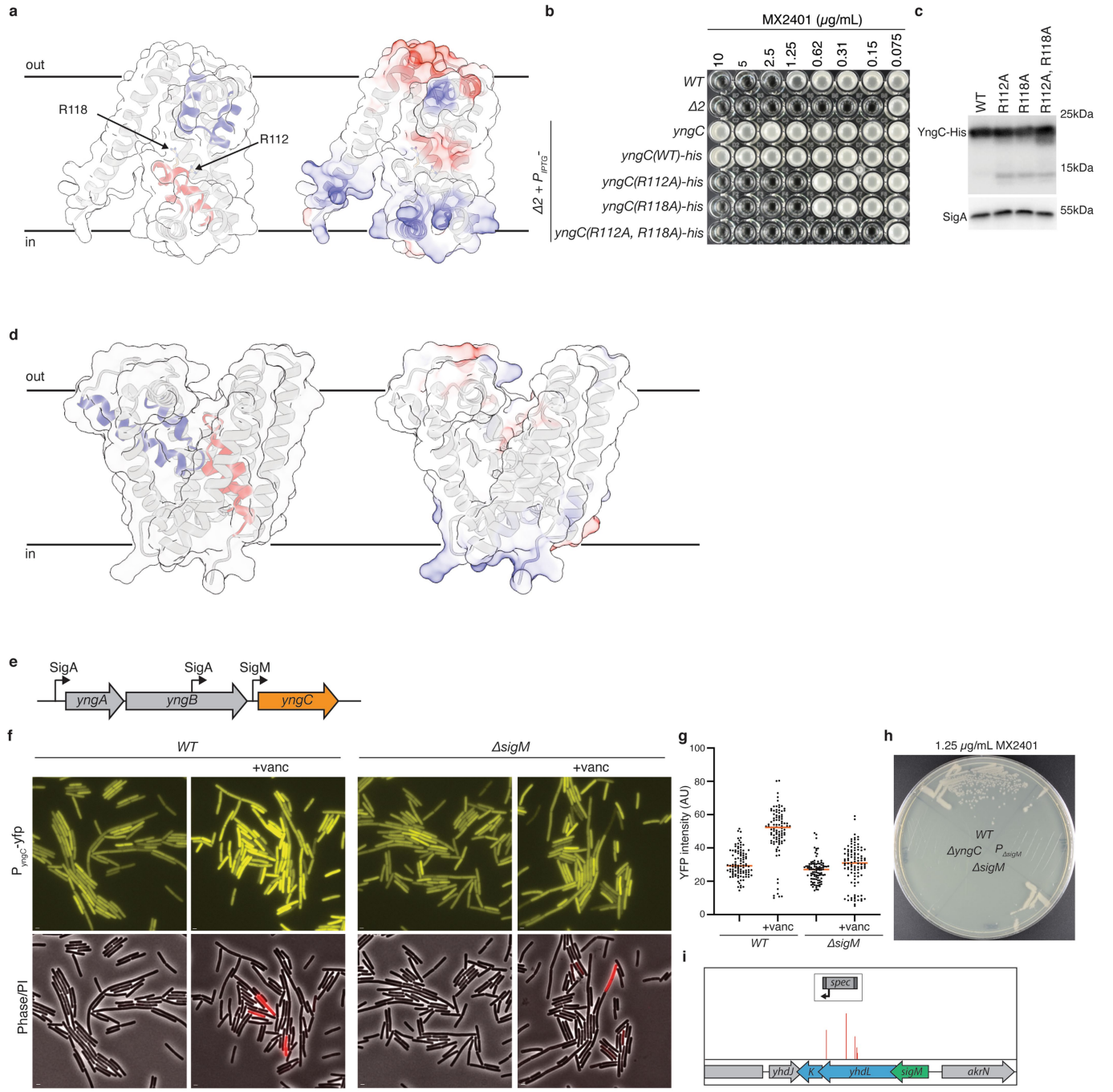

Extended Data Fig. 2 | YngC has features of membrane transporters and is expressed under σ^M control. Structural models of YngC (**a**) and SAOUHSC_00846 (**d**) as predicted by AlphaFold2. (Left) Membrane re-entrant helices are highlighted in red and blue. Conserved arginines in the red re-entrant helix of YngC are indicated. (Right) Surface charge distribution in the predicted structures. (**b**) Minimum inhibitory concentration (MIC) assays of the indicated *B. subtilis* strains with point mutations in the conserved arginines in *yngC*. (**c**) Immunoblot analysis of YngC-His levels using anti-His antibodies of the strains in (b). SigA is the sample processing control. (**e**) Schematic of the *yngABC* operon highlighting the promoters that regulate *yngC* expression. Two are recognized by sigma factor A (σ^A) and one is recognized by the ECF sigma factor M (σ^M). (**f**) Representative fluorescence images of cells harboring a transcriptional fusion of the *yngC* σ^M promoter to *yfp*. YFP fluorescence increases in cells exposed to vancomycin for 30 min, a condition that activates σ^M. The reporter is not induced by vancomycin in a *ΔsigM* mutant. Scale bar, 1 μm. (**g**) Quantification of YFP fluorescence from 100 cells of the strains and conditions in (f). Bar represents the median. (**h**) Streaks of the indicated strains on LB agar supplemented with 1.25 μg/mL MX2401. $P_{\Delta sigM}$ contains a deletion of the σ^M promoter of *yngC*. (**i**) The Tn-seq screen for MX2401 resistance mutants identified insertions in the genes (*yhdL* and *yhdK*) encoding the anti-σ^M factors, consistent with increased σ^M-dependent transcription of *yngC* providing MX2401 resistance. Transposon insertion profile at the indicated *B. subtilis* genomic region is shown. Each vertical line indicates an insertion site; its height reflects the number of reads at this position (maximum height ≥5,000). The transposon insertion site with the maximum number of reads in this region had 2,600 reads. For comparison, the insertion sites adjacent to *yngC* had >20,000 reads.

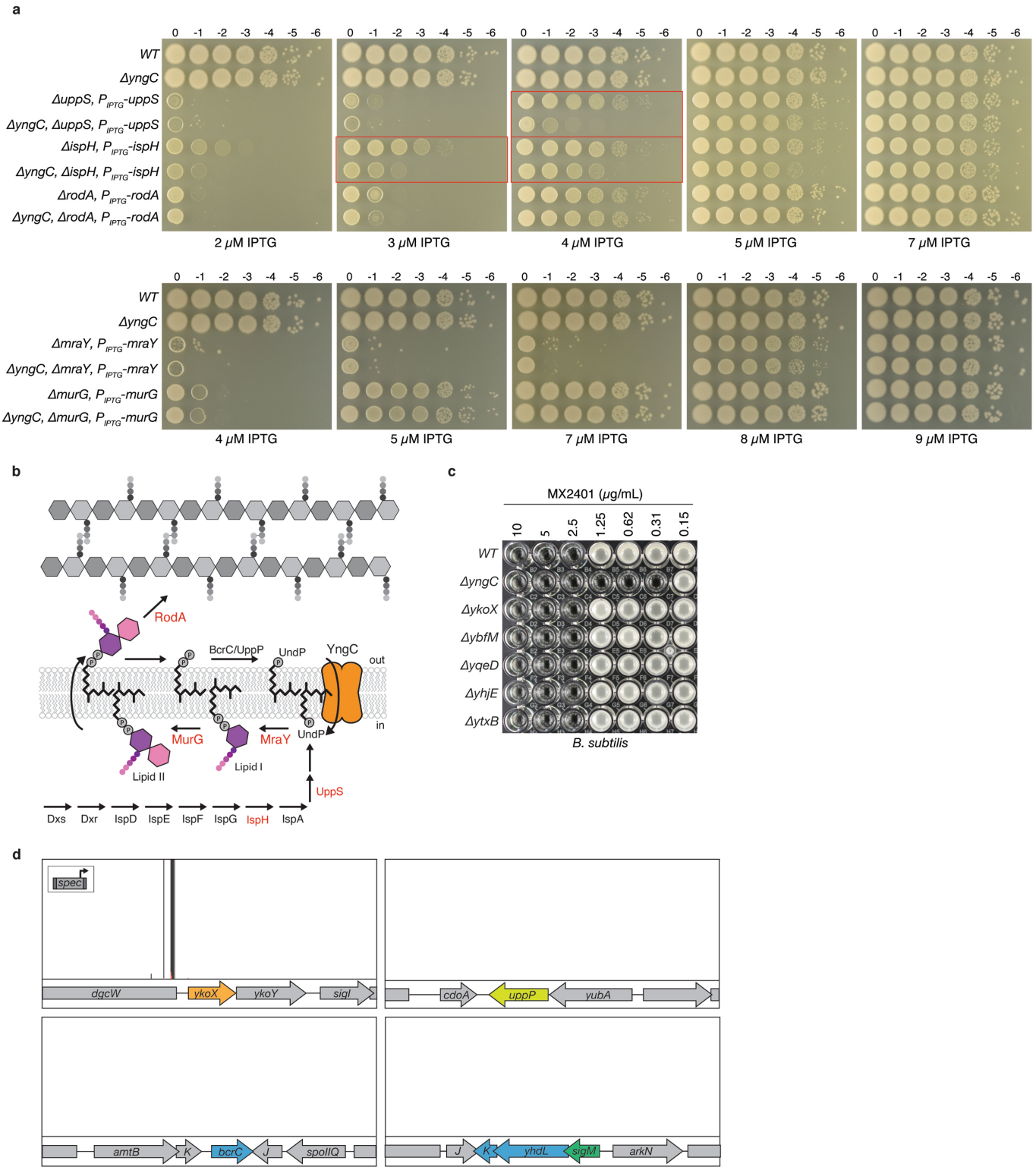

Extended Data Fig. 3 | See next page for caption.

Extended Data Fig. 3 | Δ*yngC* sensitizes *B. subtilis* to reduced levels of UndP synthesis. (**a**) Spot-dilutions of the indicated *B. subtilis* strains with IPTG-regulated alleles on LB agar supplemented with the indicated concentrations of IPTG. Strains with reduced levels of IspH or UppS are sensitive to the absence of *yngC*. Relevant comparisons are boxed in red. Strains with reduced levels of RodA, MurG or MraY grow similarly in the presence or absence of *yngC*. (**b**) Schematic of the UndP synthesis pathway illustrating the two sources of UndP for lipid II biogenesis: *de novo* synthesis and recycling. Enzymes shown in red were expressed at reduced levels in the assays in (a). (**c**) Minimum inhibitory concentration (MIC) of MX2401 in the indicated *B. subtilis* strains, each lacks one of the six DedA paralogs. (**d**) The *B. subtilis* Δ*yngC* mutant was mutagenized with a transposon carrying a strong outward facing P_{pen} promoter (insert). The library was plated on LB agar supplemented with 0.3 μg/mL MX2401 to select for mutants that provide resistance. Transposon insertion profiles at the indicated *B. subtilis* genomic regions are shown. Each vertical line indicates an insertion site; its height reflects the number of sequencing reads at this position (maximum height ≥5000). The average number of reads was >40,000. The majority of insertions mapped upstream of the *ykoX* gene in an orientation that would increase its transcription. Transposon insertions were not enriched upstream of *bcrC* or *uppP* that encode UndPP phosphatases, suggesting that these proteins do not have UndP transport activity, as was proposed previously[3,38]. Unlike the Tn-seq screen in a wild-type (*yngC*+) background, in the Δ*yngC* mutant, transposon insertions were not enriched in the genes (*yhdL* and *yhdK*) encoding the anti-σ^M factors, consistent with the model that their inactivation provides increased MX2401 resistance by increasing σ^M-dependent transcription of *yngC*.

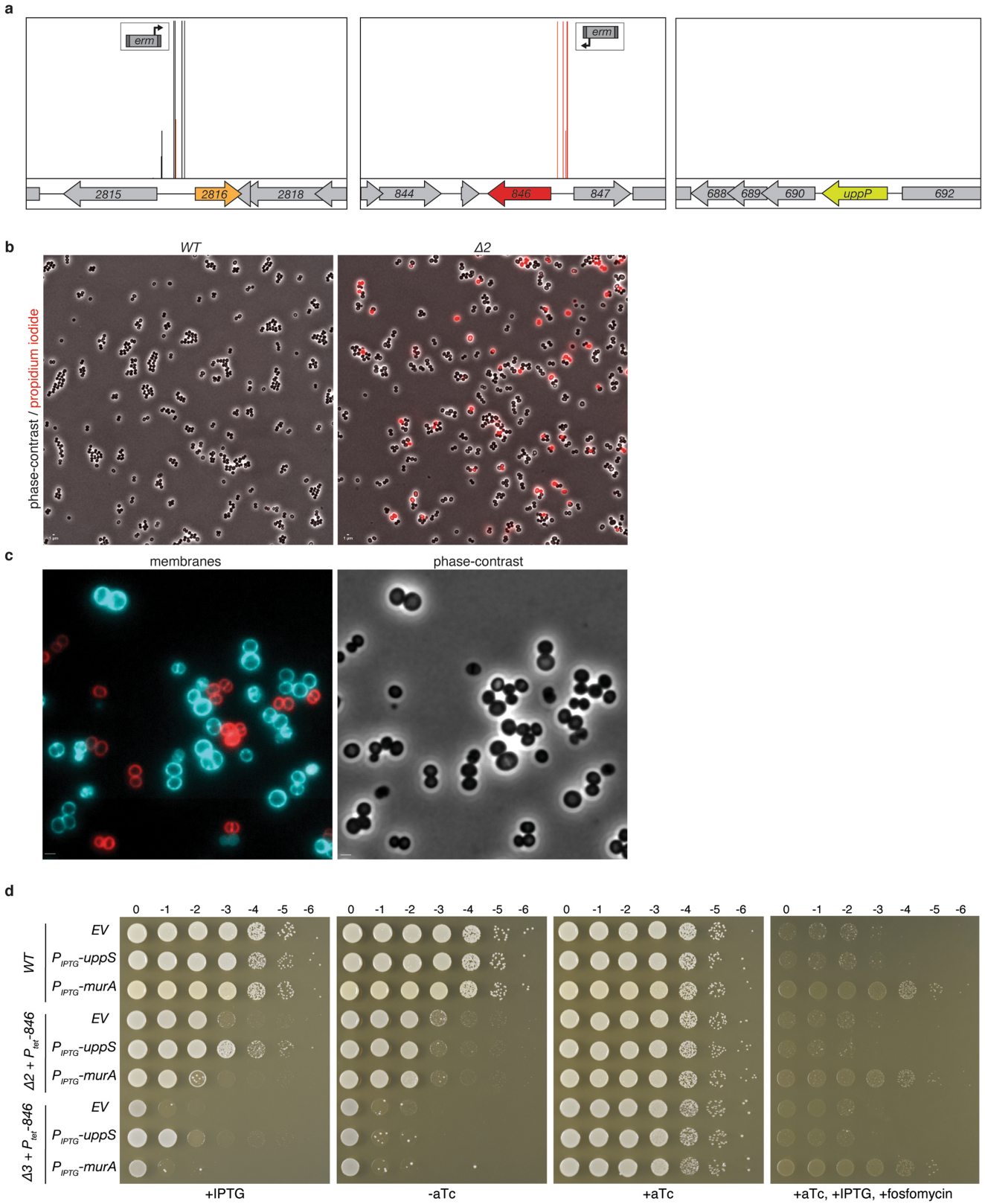

Extended Data Fig. 4 | See next page for caption.

Extended Data Fig. 4 | A transposon-sequencing screen identified insertions upstream of *02816* and *00846* that confer resistance to amphomycin in *S. aureus*. (**a**) Reanalysis of Tn-seq data from *Santiago et al*. 2018[16]. A library of *S. aureus* mutagenized with a transposon carrying a strong outward facing promoter (P_{tuf}) was grown in sub-inhibitory concentrations of amphomycin (9.6 µg/mL). Transposon insertion profiles at the indicated *S. aureus* genomic regions are shown. Each vertical line indicates an insertion site; its height reflects the number of reads at this position (maximum height ≥2,000). Most transposon insertions mapped upstream of *SAOUHSC_02816* and *SAOUHSC_00846* in orientations that are predicted to increase transcription of these genes. By contrast, insertions were not enriched upstream of the UndPP phosphatase *uppP*, suggesting that this membrane phosphatase does not have UndP transport activity, as previously proposed[3,38]. (**b**) Representative micrographs of wild-type and the Δ2 (Δ*uptA* Δ*popT*) double mutant. Shown are overlays of phase-contrast and fluorescence images of propidium iodide-stained cells. Quantification of the PI-positive cells from several fields of view (>1,000 cells per strain) yielded a PI-positive rate of 0.1% for wild-type and 10% for the Δ*uptA* Δ*popT* mutant. (**c**) Wild-type and Δ2 cells were stained with fluorescent membrane dyes FM-464 (red) and TMA-DPH (blue), respectively, and then mixed and imaged on the same agarose pad. Scale bar, 1 µm. (**d**) Spot-dilutions of the indicated *S. aureus* strains harboring an empty vector (EV) or a vector with an IPTG-regulated promoter fused to *uppS* or *murA*. The Δ2 *(Δ00846 Δ02816)* and Δ3 *(Δ00846 Δ02816 Δ00901)* strains have an aTc-regulated allele of *00846* (846). In the presence of 500 µM IPTG the Δ2 strain overexpressing UppS grows similarly to wild-type and the Δ3 strain is able to form tiny colonies at all dilutions. By contrast, the growth of the two mutants overexpressing MurA phenocopies the mutants with the empty vector. Overexpression of MurA enables growth on LB agar plates supplemented with 3 µg/mL fosfomycin.

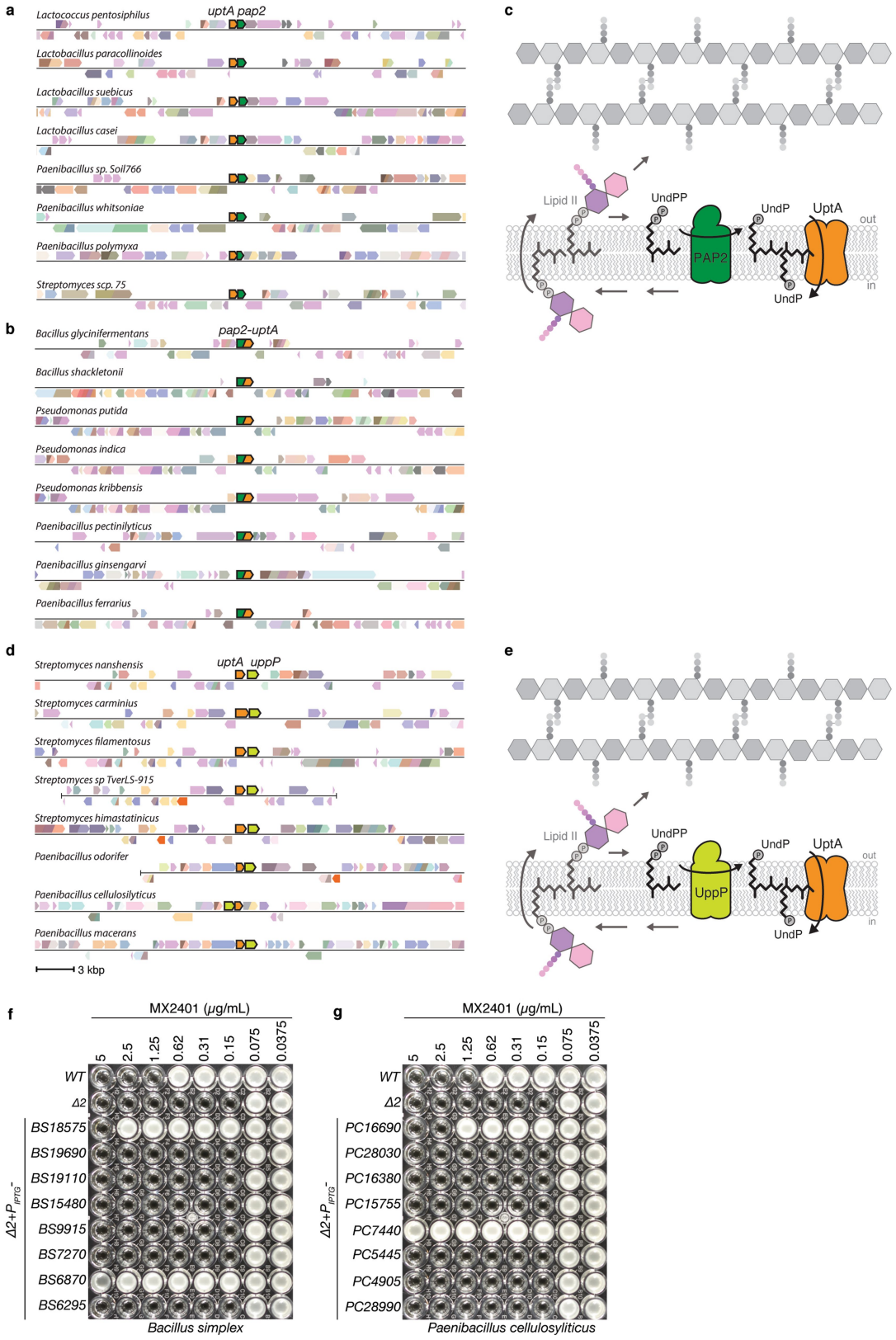

Extended Data Fig. 5 | See next page for caption.

Extended Data Fig. 5 | Gene neighborhood analyses reveal that *dedA* paralogs can be found adjacent to or fused with *pap2* lipid phosphatases or adjacent to *uppP* undecaprenyl-pyrophosphate phosphatases. Representative genomic neighborhood analyses showing synteny (**a**) and gene-fusions (**b**) of DedA family members with PAP2 lipid phosphatases. (**c**) Schematic of the lipid II cycle highlighting the role of PAP2 family members like BcrC and DedA family members like YngC (UptA) in dephosphorylating UndPP and flipping UndP across the membrane, respectively. (**d**) Representative genomic neighborhood analysis showing synteny of *dedA* transporters with the undecaprenyl-pyrophosphate phosphatase *uppP*. Most examples of synteny between *dedA* and *uppP* genes are from *Streptomycetes* and *Paenibacilli* genomes. (**e**) Schematic of the lipid II cycle highlighting the role of UppP family members and DedA family members like YngC (UptA) in dephosphorylating UndPP and flipping UndP across the membrane, respectively. MIC assays of the indicated *B. subtilis* strains lacking *uptA* and *ykoX* (Δ2) expressing one of the eight *Bacillus simplex* (**f**) or *Paenibacillus cellulosyliticus* (**g**) DedA paralogs. *BS18575* is adjacent to a *pap2* gene in *B. simplex*. *PC16690* is adjacent to a *uppP* gene in *P. cellulosyliticus*. Strains were grown in LB with 500 μM IPTG in the presence of the indicated concentration of MX2401. Uniprot IDs for the proteins included in the genome neighborhood diagrams can be found in Supplementary Table 3.

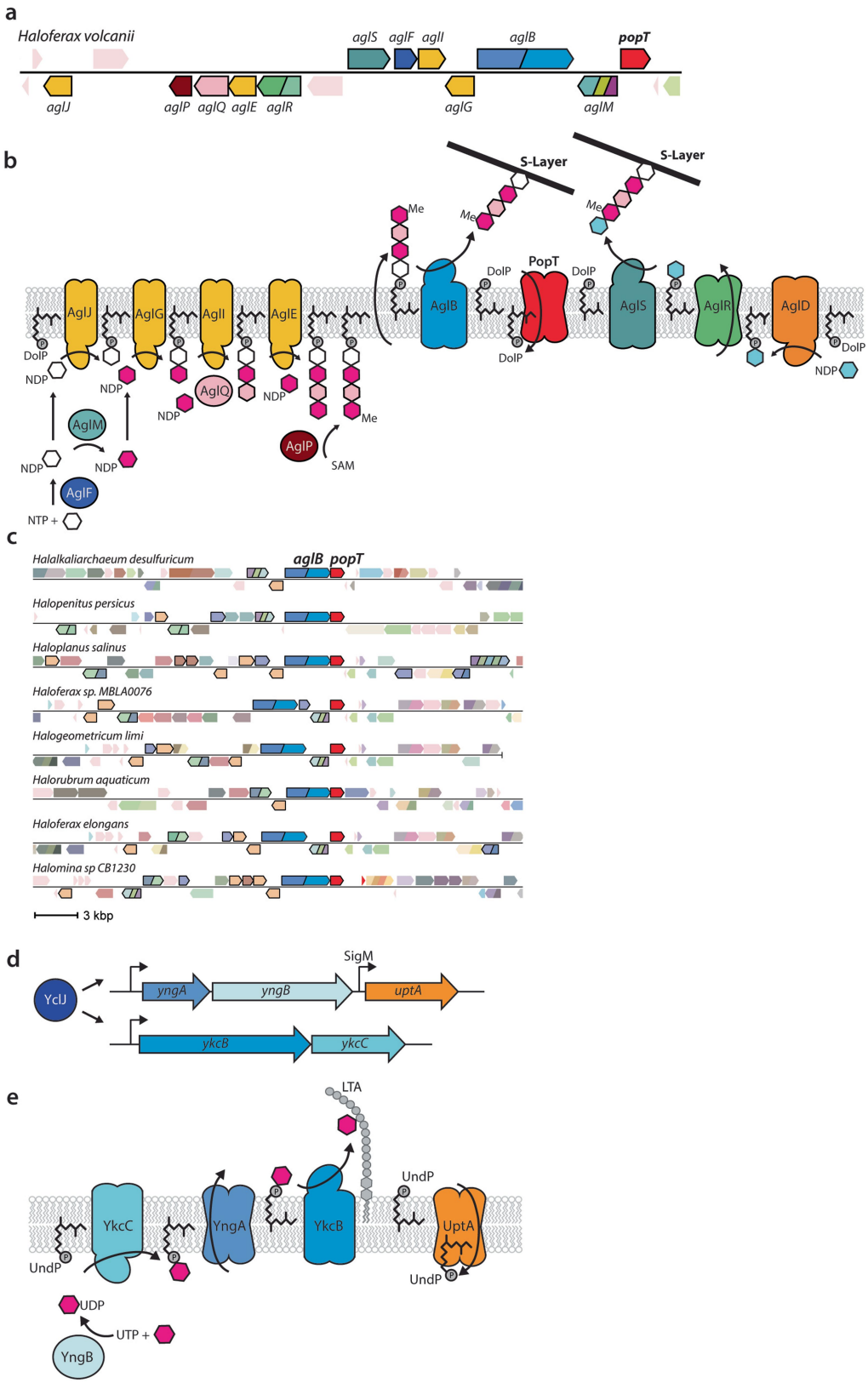

Extended Data Fig. 6 | See next page for caption.

Extended Data Fig. 6 | Gene neighborhood analysis indicates that *duf368* genes are often present in archaeal gene clusters involved in S-layer protein glycosylation. (**a**) Representative genomic neighborhood from *Haloferax volcanii* with all the characterized genes involved in S-layer protein glycosylation and *popT* highlighted. (**b**) Schematic of the S-layer protein glycosylation pathway encoded in the *H. volcanii* gene cluster as described in ref. [26]. PopT is hypothesized to catalyze the recycling of DolP to complete the cycle. AglR is shown flipping one of the two UndP-linked sugars but could transport both. (**c**) Gene neighborhood analysis showing synteny of *duf368* (*popT*) transporters with *aglB* and other genes involved in N-linked protein glycosylation (outlined in black). Uniprot IDs for the proteins included in this diagram can be found in Supplementary Table 3. (**d**) Cartoon depiction of the regulation of the *yngABC* and *ykcBC* operons by the transcription factor YclJ[54]. (**e**) Schematic of the putative cell surface glycosylation pathway encoded by YclJ regulon members[27]. YngA is a member of the GtrA flippase family that transports UndP-linked monosaccharides across the cytoplasmic membrane. YngB is a member of the UDP glucose pyrophosphorylase family and has been shown to charge sugars with UDP groups[27]. YkcB is a member of the glycosyltransferase-39 family that transfers monosaccharides from the UndP carrier to surface polymers and is thought to glycosylate lipoteichoic acid (LTA). YkcC is a member of the glycosyltransferase-2 family that adds UDP charged monosaccharides onto UndP on the cytoplasmic leaflet of the membrane. The DedA paralog YngC (UptA) is proposed to complete the cycle.

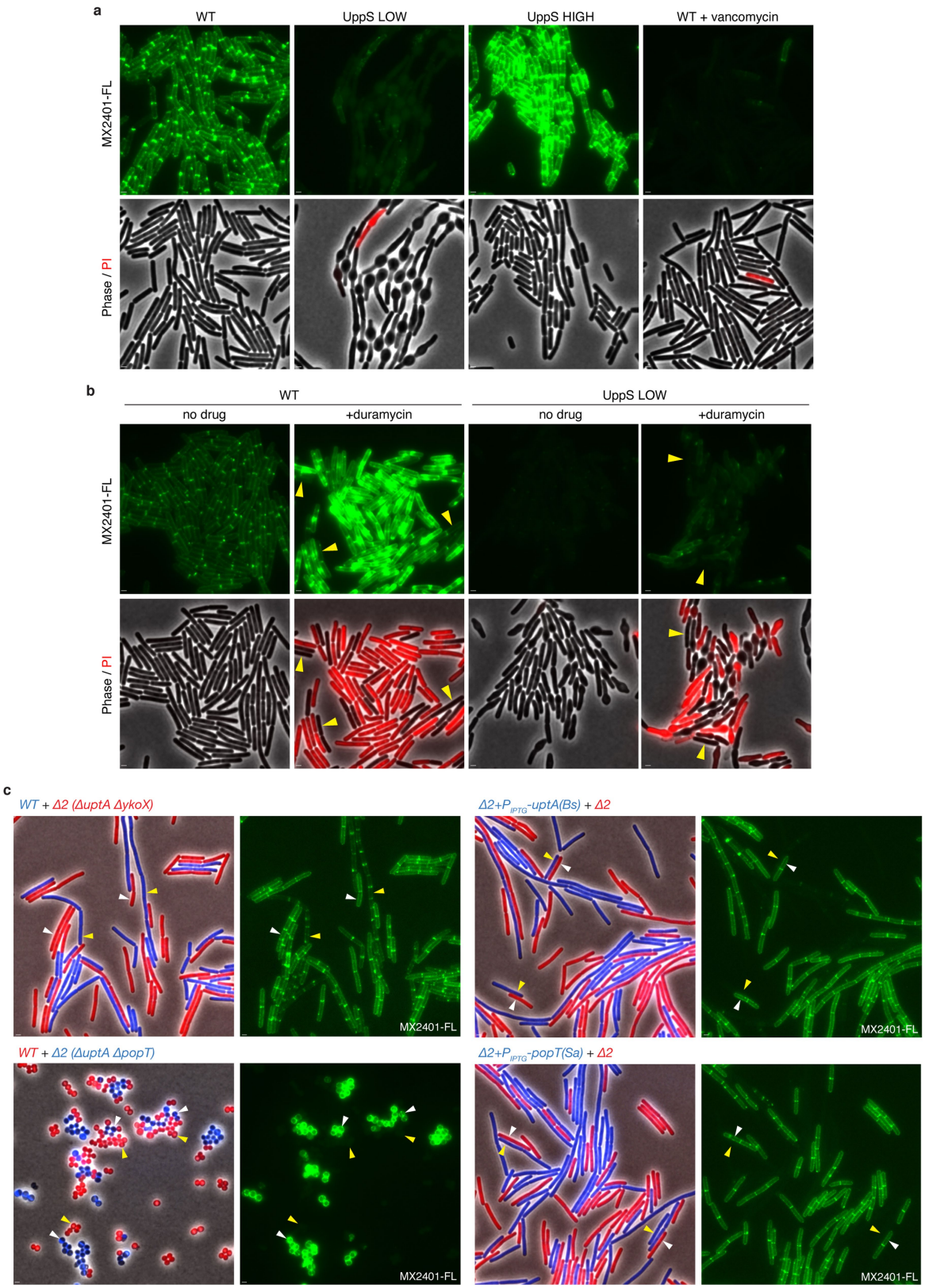

Extended Data Fig. 7 | See next page for caption.

Extended Data Fig. 7 | MX2401-FL specifically labels outward-facing UndP. (**a**) Validation of MX2401 conjugated to CF488 (MX2401-FL). Representative fluorescence and phase-contrast images of the indicated strains labeled with MX2401-FL and propidium iodide (PI). Cells with reduced *de novo* synthesis of UndP (UppS LOW) harbor an IPTG-regulated allele of *uppS* (Pspank-*uppS*) and were propagated in the presence of 4 μM IPTG. Cells with increased *de novo* synthesis of UndP (UppS HIGH) harbor a stronger IPTG-regulated allele of *uppS* (Physpank-*uppS*) and were propagated with 500 μM IPTG. UppS LOW cells have low MX2401-FL staining and bulge due to impaired for cell wall synthesis. UppS HIGH cells have high MX2401-FL staining and are shorter. Cells treated with vancomycin for 5 min prior to MX2401-FL staining trap UndP in lipid II and have low MX2401-FL signal. All MX2401-FL images were normalized identically with minimum and maximum intensities of 125 and 600 to detect weak MX2401-FL staining in the UppS LOW and vancomycin-treated strains. (**b**) Wild-type and UppS LOW strains were stained with MX2401-FL or a mixture of MX2401-FL and duramycin, which generates pores in the membrane allowing MX2401-FL access to the cytoplasmic-facing UndP. Cells with membrane permeability defects as assayed by PI have higher MX2401-FL signal. Cells with intact membranes (yellow carets) have lower MX2401-FL staining. All MX2401-FL images were normalized identically with minimum and maximum intensities of 125 and 1500 to prevent saturating the MX2401-FL signal. (**c**) Representative microscopy images of the indicated strains. Strains expressing different fluorescent proteins (*B. subtilis*) or labeled with different fluorescent D-amino acids (*S. aureus*) were mixed and then stained with MX2401-FL. (Left) overlays of phase contrast and fluorescent images in the red and blue channels to distinguish the two strains. (Right) MX2401-FL staining. Yellow carets highlight wild-type cells or cells over-expressing UptA(*Bs*) or PopT(*Sa*). White carets highlight cells lacking the UndP transporters. Scale bar, 1 μm.

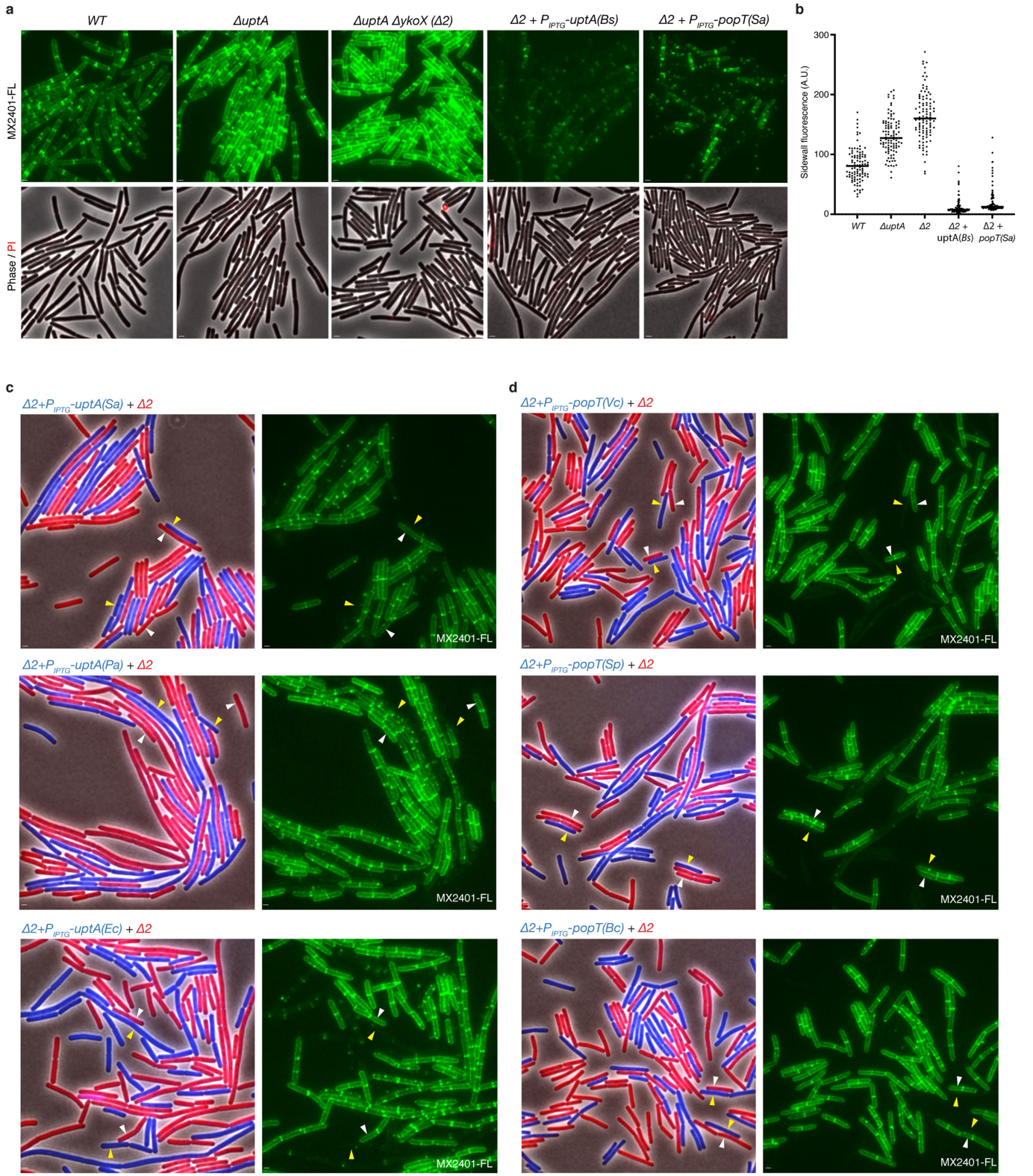

Extended Data Fig. 8 | UptA and PopT expression reduces MX2401-FL surface labeling. (**a**) Representative fluorescence and phase-contrast images of the indicated *B. subtilis* strains labeled with MX2401-FL and propidium iodide. The strains with IPTG-regulated *popT* and *uptA* alleles were grown in the presence of 500 µM IPTG. (**b**) Quantification of MX2401-FL labeling from the strains imaged in (a). Fluorescence intensity measurements of the sidewalls of 100 cells of each genotype were determined and plotted. Bar represents the median. (**c**) Representative images of the indicated *B. subtilis* strains. Two strains expressing different fluorescent proteins were mixed and then stained with MX2401-FL. The left panels show overlays of phase contrast and fluorescent images in the red and blue channels to distinguish the two strains. The right panels show MX2401-FL staining. Yellow carets highlight cells over-expressing an UptA homolog from *S. aureus* (*Sa*), *Pseudomonas aeruginosa* (*Pa*), and *E. coli* (*Ec*) in a strain lacking *uptA* and *ykoX* (Δ2). White carets highlight cells lacking *uptA* and *ykoX*. (**d**) Yellow carets highlight cells over-expressing a PopT homolog from *Vibrio cholerae* (*Vc*), *Streptococcus pneumoniae* (*Sp*), or *Bacillus cereus* (*Bc*) in a strain lacking *uptA* and *ykoX* (Δ2). White carets highlight cells lacking *uptA* and *ykoX*. Scale bar, 1 µm.

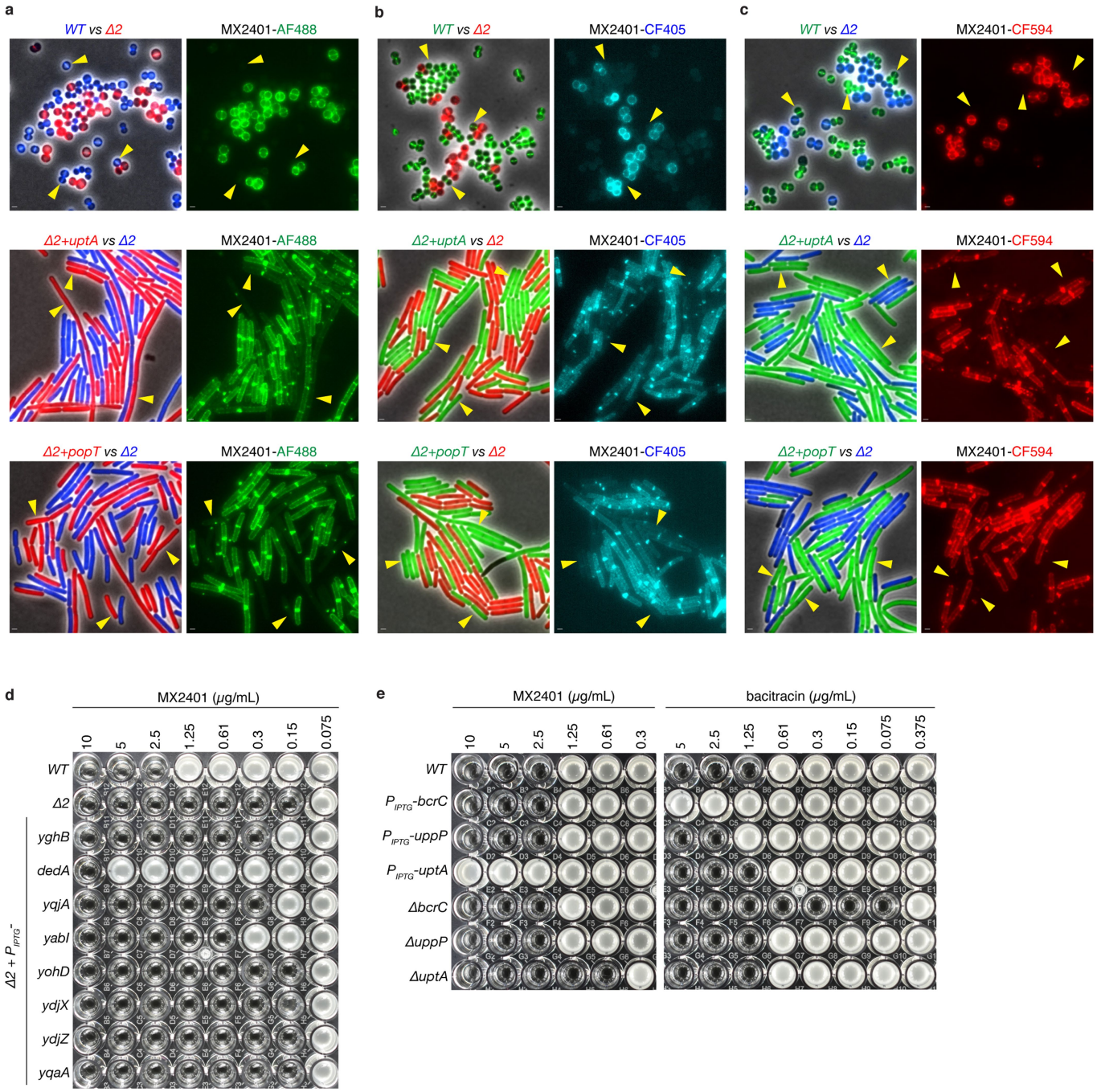

Extended Data Fig. 9 | MX2401 conjugated to three different fluorescent dyes stains cells similarly. Representative images of the indicated *B. subtilis* or *S. aureus* strains. Two strains expressing different fluorescent proteins (*B. subtilis*) or labeled with different fluorescent D-amino acids (*S. aureus*) were mixed and then stained with MX2401 labeled with (**a**) Alexa Fluor 488 (MX2401-AF488), (**b**) CF405 (MX2401-CF405), and (**c**) CF594 (MX2401-CF594). Alexa Fluor 488 prevents membrane permeation of its conjugates[30,31]. CF405 and CF594 are also reported to be membrane-impermeable by the manufacturer (Biotium). The left panels show overlays of phase-contrast and fluorescence images in the red and blue, red and green, or green and blue channels to distinguish the two strains. The right panels show MX2401-FL staining. Yellow carets highlight wild-type cells or cells over-expressing UptA*(Bs)* or PopT*(Sa)*. All three fluorescently labeled MX2401 probes yield similar results. Scale bar, 1 μm. (**d**) MIC assays of the indicated strains each expressing one of the eight *E. coli* DedA paralogs in *B. subtilis* lacking *uptA* and *ykoX* (Δ2). Strains were grown in LB with 10 μM IPTG. At 500 μM, cells expressing YqjA and YabI had 4-fold higher MICs (≥8-fold lower than cells expressing DedA). (**e**) Over-expression or deletion of the undecaprenyl-pyrophosphate phosphatase genes *uppP* or *bcrC* in *B. subtilis* do not alter the MIC of MX2401. MIC assays of the indicated *B. subtilis* strains tested with MX2401 and separately with bacitracin that targets UndPP. These experiments were performed in a strain background deleted for the bacitracin efflux pump (Δ*bceAB*).

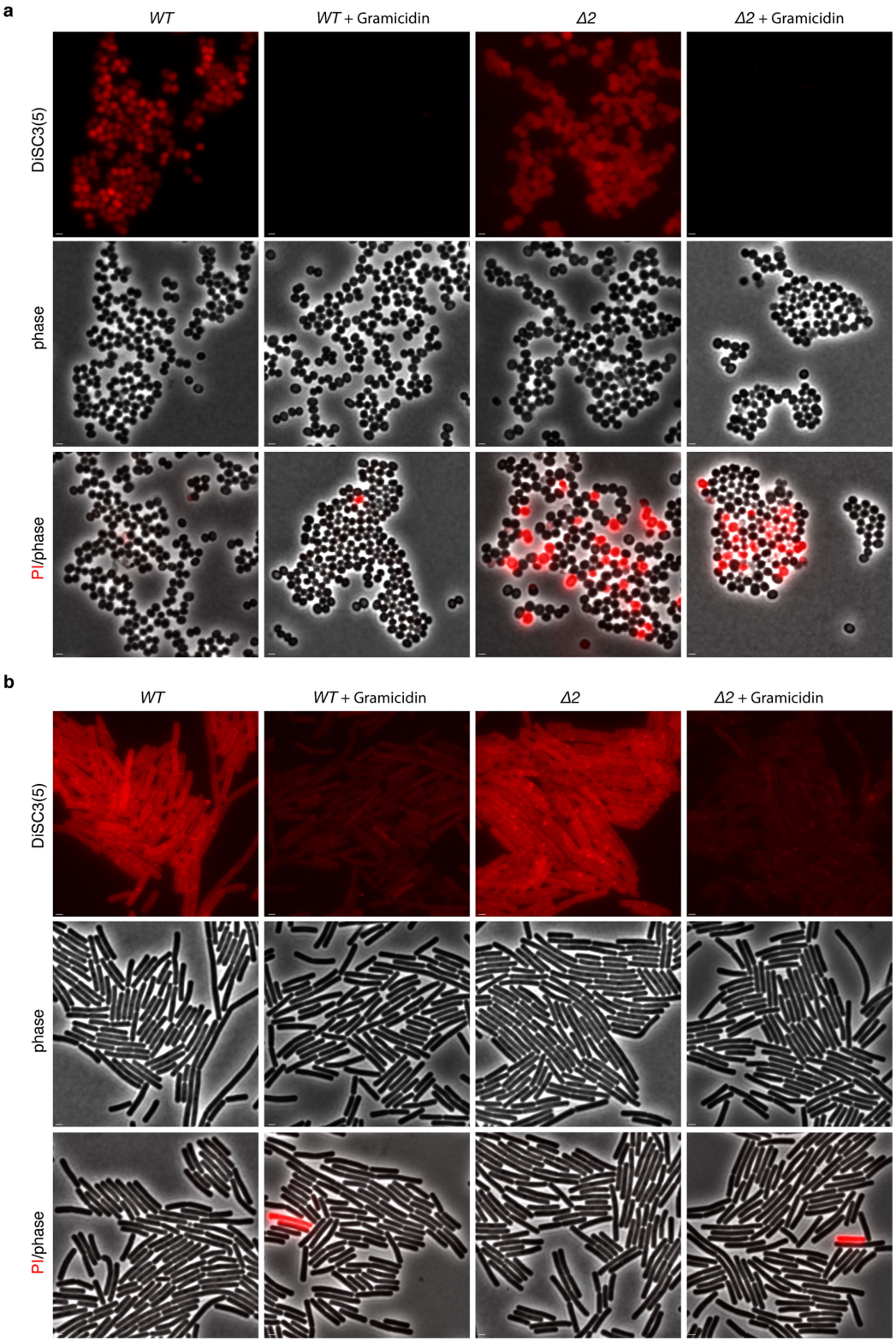

Extended Data Fig. 10 | *S. aureus* and *B. subtilis* cells lacking UndP transporters remain polarized. (**a**) Representative fluorescence and phase-contrast images of *S. aureus* wild-type and the *ΔpopT ΔuptA* (Δ2) mutant. The two strains were stained with the potentiometric dye 3,3′-Dipropylthiadicarbocyanine Iodide (DiSC3(5)). Treatment with the ionophore Gramicidin that depolarizes membranes was used as a positive control. The same cultures were separately stained with propidium iodide (PI) to assess the percentage of cells with membrane permeability defects. (**b**) Representative images of wild-type and the *ΔuptA ΔykoX* (Δ2) *B. subtilis* mutant stained with DiSC3(5). Gramicidin was used as a positive control for loss of membrane potential. Scale bar, 1 µm.

nature portfolio

Corresponding author(s): David Rudner

Last updated by author(s): Apr 11, 2022

Reporting Summary

Nature Portfolio wishes to improve the reproducibility of the work that we publish. This form provides structure for consistency and transparency in reporting. For further information on Nature Portfolio policies, see our Editorial Policies and the Editorial Policy Checklist.

Statistics

For all statistical analyses, confirm that the following items are present in the figure legend, table legend, main text, or Methods section.

n/a	Confirmed	
☐	☒	The exact sample size (*n*) for each experimental group/condition, given as a discrete number and unit of measurement
☒	☐	A statement on whether measurements were taken from distinct samples or whether the same sample was measured repeatedly
☒	☐	The statistical test(s) used AND whether they are one- or two-sided *Only common tests should be described solely by name; describe more complex techniques in the Methods section.*
☒	☐	A description of all covariates tested
☒	☐	A description of any assumptions or corrections, such as tests of normality and adjustment for multiple comparisons
☐	☒	A full description of the statistical parameters including central tendency (e.g. means) or other basic estimates (e.g. regression coefficient) AND variation (e.g. standard deviation) or associated estimates of uncertainty (e.g. confidence intervals)
☒	☐	For null hypothesis testing, the test statistic (e.g. *F*, *t*, *r*) with confidence intervals, effect sizes, degrees of freedom and *P* value noted *Give P values as exact values whenever suitable.*
☒	☐	For Bayesian analysis, information on the choice of priors and Markov chain Monte Carlo settings
☒	☐	For hierarchical and complex designs, identification of the appropriate level for tests and full reporting of outcomes
☒	☐	Estimates of effect sizes (e.g. Cohen's *d*, Pearson's *r*), indicating how they were calculated

Our web collection on statistics for biologists contains articles on many of the points above.

Software and code

Policy information about availability of computer code

Data collection	Microscopy data collection was performed using Nikon Elements 4.3 software.
Data analysis	Microscopy data analysis was performed using Image J (version 2.3) software. All graphs were generated in GraphPad Prism 9. Multiple sequence alignments were generated using the publicly available software Clustal Omega version 1.2.4, available at:https://www.ebi.ac.uk/Tools/msa/clustalo/ and visualized with Espript 3.0, available at:https://espript.ibcp.fr/ESPript/cgi-bin/ESPript.cgi Gene neighborhood analysis was performed using publicly available software from the Enzyme Function initiative including the Enzyme Similarity Tool (EFI-EST v2.0) and the Genome Neighborhood Tool (EFI-GNT v1.0), available at:https://efi.igb.illinois.edu/. Dendrograms were made using the publicly available software AnnoTree version 1, available at: http://annotree.uwaterloo.ca/. Bowtie 1.0.0 was used to map transposon insertion sites to the Bacillus subtilis genome (NCBI NC_00964.3). Chimera X1.3 was used for protein structure analysis.

For manuscripts utilizing custom algorithms or software that are central to the research but not yet described in published literature, software must be made available to editors and reviewers. We strongly encourage code deposition in a community repository (e.g. GitHub). See the Nature Portfolio guidelines for submitting code & software for further information.

Data

Policy information about availability of data

All manuscripts must include a data availability statement. This statement should provide the following information, where applicable:

- Accession codes, unique identifiers, or web links for publicly available datasets
- A description of any restrictions on data availability
- For clinical datasets or third party data, please ensure that the statement adheres to our policy

NGS datasets generated in this study have been uploaded to the NCBI Sequence read archive within project PRJNA898639 (SAMN31619234 and SAMN31619233). Reads were mapped to B. subtilis genome (NCBI NC_00964.3). NGS datasets that were reanalyzed from Santiago et al. 2018 can be found on the NCBI Sequence read archive (SRX3390726) and the analysis was conducted as described in the paper. Raw data for all graphs has been uploaded as source data. Uniprot accession codes for gene neighborhood analysis can be found in supplementary tables. Primers, synthetic DNA constructs and strains used can be found in supplementary tables.

Field-specific reporting

Please select the one below that is the best fit for your research. If you are not sure, read the appropriate sections before making your selection.

☒ Life sciences ☐ Behavioural & social sciences ☐ Ecological, evolutionary & environmental sciences

For a reference copy of the document with all sections, see nature.com/documents/nr-reporting-summary-flat.pdf

Life sciences study design

All studies must disclose on these points even when the disclosure is negative.

Sample size	For microscopy experiments, no sample size calculations were calculated. All analyses were performed on an arbitrarily large number of cells that was representative of the population. All fluorescence quantifications were performed on greater than 100 cells, from multiple fields of view and all data-points are presented. This is standard for the field. All other experiments involve bulk assays using greater than 10^7 cells and were performed in at least triplicate.
Data exclusions	No data excluded.
Replication	All MIC experiments were performed in at least biological triplicate and representative images are shown. All microscopy analyses were performed in at least biological duplicate with many fields of view analyzed and representative images are shown. Spot assays and streak analysis were performed in at least biological triplicate. Western blotting was performed in biological duplicate. Attempts at replication for all experiments was successful.
Randomization	We did not randomize samples, as after experimental setup, all measurements and analysis were performed identically across all conditions.
Blinding	We did not blind samples, as after experimental setup, all measurements and analysis were performed identically across all conditions.

Reporting for specific materials, systems and methods

We require information from authors about some types of materials, experimental systems and methods used in many studies. Here, indicate whether each material, system or method listed is relevant to your study. If you are not sure if a list item applies to your research, read the appropriate section before selecting a response.

Materials & experimental systems

n/a	Involved in the study
☐	☒ Antibodies
☒	☐ Eukaryotic cell lines
☒	☐ Palaeontology and archaeology
☒	☐ Animals and other organisms
☒	☐ Human research participants
☒	☐ Clinical data
☒	☐ Dual use research of concern

Methods

n/a	Involved in the study
☒	☐ ChIP-seq
☒	☐ Flow cytometry
☒	☐ MRI-based neuroimaging

Antibodies

Antibodies used	1) THE™ His Tag Antibody (used at 1:4000), mAb, Mouse, Genscript, Cat A00186, Clone 6G2A9 2) Anti-SigA (used at 1:10000), polyclonal, Gift of Masaya Fujita (University of Houston)

3) Goat Anti-Mouse IgG (H + L)-HRP Conjugate #1706516 (Used at 1:20000), BioRad.
4) Goat Anti-Rabbit IgG (H + L)-HRP Conjugate #1706515 (Used at 1:3000), BioRad.

Validation

The His Tag antibody has been used numerous times in other publications and validation is available on the company website, available at: https://www.genscript.com/antibody/A00186-THE_His_Tag_Antibody_mAb_Mouse.html
The anti-sigA antibody was generated by Masaya Fujita and has been used in numerous publications as a loading control for B. subtilis in studies originating from our lab and others. Specificity of anti-SigA antibodies were confirmed with purified SigA protein and using lysates from B. subtilis cell expressing different levels of SigA under IPTG control.